RNA Folding Topology and Intermolecular Contacts in the AMP−RNA Aptamer Complex†

Feng Jiang, Radovan Fiala, David Live, R. Ajay Kumar, and Dinshaw J. Patel*

Cellular Biochemistry and Biophysics Program, Memorial Sloan-Kettering Cancer Center, New York, New York 10021

Received June 6, 1996; Revised Manuscript Received July 29, 1996⊗

ABSTRACT: We report below on the NMR structural characterization of the complex between AMP and a 40-mer RNA aptamer in aqueous solution. Resonance assignments are based on multinuclear multidimensional NMR studies on complexes uniformly ^{13}C,^{15}N-labeled with either AMP or the RNA aptamer. AMP binds to an internal loop (labeled G7-G8-A9-A10-G11-A12-A13-A14-C15-U16-G17) and bulge (G34 positioned opposite the internal loop) segment in the RNA aptamer, and our NMR study provides insights into features of the RNA folding topology and the molecular recognition events in the AMP binding pocket on the RNA. Specifically, the helical stems are extended by G·G mismatch formation from either direction into the internal loop/bulge segment of the RNA aptamer on complex formation. The internal loop adopts a unique fold with the purine ring of AMP intercalated between A10 and G11 in the complex. The G8-A9-A10-AMP segment adopts certain stacking features in common with a GNRA turn and is closed by the G7·G11 mismatch pair. The purine rings of A12 and G34 (syn) are stacked on each other and participate in stablizing the AMP intercalation site. A large number of intermolecular NOEs have been identified between the AMP ligand and the G8, A10, G11, G17, U18, and G34 residues on the RNA aptamer in the complex. The Watson−Crick edge of the AMP is oriented toward the exocyclic amino group of G8, suggestive of a hydrogen-bonding alignment between G8 and AMP in the complex. The AMP sugar ring is positioned in the minor groove of the rightward helical stem centered about the G17·G34 mismatch and U18·A33 Watson−Crick pairs. The AMP binds to one face of the folded internal loop/bulge segment of the RNA aptamer while the opposite face is capped by a stacked alignment of the A13-A14-C15-U16 segment located toward the 3′-end of the internal loop segment. Globally, the two helical stems of the RNA aptamer are aligned approximately orthogonal to each other with tertiary interactions centered about the internal loop/bulge segment generating the AMP binding site on the RNA.

RNA is unique among biological macromolecules in that it exhibits coding, information transfer, and catalytic activities [reviewed in Gesteland and Atkins (1993)]. RNA participates in a diverse array of biological phenomena, and this functional diversity reflects its ability to adopt a range of folding topologies [reviewed in Nagai and Mattaj (1994)]. Little is known about the complex structural scaffolds adopted by RNA molecules and the details of substrate binding sites so critical for their catalytic function. Our laboratory has addressed issues related to RNA structure and recognition in solution by focusing on ligand−RNA aptamer complexes. *In vitro* selection and *in vitro* evolution techniques utilizing random sequence RNA libraries (Robertson & Joyce, 1990; Ellington & Szostak, 1990; Tuerk & Gold, 1990) have identified RNA aptamer sequences that target ligands ranging from cofactors to antibiotics and peptides [reviewed in Joyce (1994), Chapman and Szostak (1994), and Burgstaller and Famulok (1995)]. These RNA aptamers exhibit both high binding affinity and an ability to discriminate between the target ligands and their closely related analogs.

High-resolution multinuclear multidimensional NMR is a technique ideally suitable for the structural characterization of medium molecular weight (in the 30−50-mer range) RNA aptamers (preferably labeled uniformly with ^{13}C and ^{15}N) complexed to their ligand targets. The RNA aptamers in these complexes can fold into compact conformations amenable to structural characterization by molecular dynamics computations guided by the NMR-derived intermolecular restraints between the ligand and the RNA. We have begun a structural program focused on applying NMR techniques [reviewed in Wyatt and Tinoco (1993), Moore (1995), and Pardi (1995)] and molecular dynamics computations to identify the molecular determinants and recognition elements in the binding of the cofactors flavin mononucleotide (Fan et al., 1996) and adenosine monophosphate (this study) to their respective RNA aptamer sites.

Recently, an RNA aptamer has been identified through *in vitro* selection that binds to ATP, AMP, and adenosine (covalently linked to an agarose column through their purine C8 position) with micromolar affinity. The RNA aptamer secondary structure **1** contains a consensus 11 base internal loop positioned opposite an invariant guanine bulge and flanked by two stem segments (Sassanfar & Szostak, 1993). The same internal loop and bulge sequence has also been observed for RNA aptamers that target the cofactor nicotine adenine dinucleotide (Burgstaller & Famulok, 1994). By contrast, the corresponding ATP binding DNA aptamer adopts a totally different secondary structure fold (Huizenga & Szostak, 1995). This ATP binding RNA aptamer has in turn been utilized as a scaffold to apply *in vitro* evolution approaches to identify new ribozymes with polynucleotide

† This research was funded from Start-up Funds to D.J.P. and by a postdoctoral fellowship to F.J. from the NIH. R.A.K. is a postdoctoral fellow of the Miriam and Benedict Wolf Cancer Research Fund.

* Corresponding author. Phone: 212-639-7207. FAX: 212-717-3066.

⊗ Abstract published in *Advance ACS Abstracts,* October 1, 1996.

S0006-2960(96)01345-1 CCC: $12.00

kinase activity (Lorsch & Szostak, 1994).

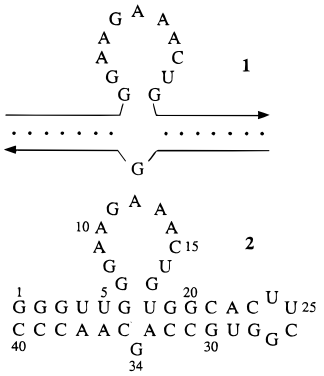

Sassanfar and Szostak (1993) have defined a minimal 40-mer RNA aptamer sequence **2** that bound ATP with a K_D of ~10 μM. The dissociation constant dropped further to 2 μM in the presence of Mg^{2+}. In this paper we report on a detailed multinuclear multidimensional NMR study that defines features of the RNA folding topology and identifies the intermolecular contacts in the AMP−RNA aptamer **2** complex. This analysis was facilitated by uniformly ^{13}C,^{15}N-labeling either the ligand or the RNA in the AMP−RNA aptamer complex. The present NMR study has provided the key intramolecular and intermolecular restraints that has in turn enabled us to define the solution structure of the AMP−RNA aptamer **2** complex (Jiang et al., 1996a).

MATERIALS AND METHODS

RNA Synthesis and Purification. The RNA aptamer **2** was synthesized by *in vitro* transcription using T7 RNA polymerase (Wyatt et al., 1991; Milligan et al., 1987; Milligan & Uhlenbeck, 1989). A DNA template (Operon, Alameda, CA), including the 17 nucleotide T7 promoter, the sequence corresponding to AMP aptamer, and two restriction sites (*Eco*RI and *Sma*I), was cloned into pUC19. Large amounts of linear pUC19 plasmid was obtained by digestion of bacteria-amplified pUC19 plasmid with *Sma*I and was used as the template for *in vitro* transcription. The T7 RNA polymerase was purified from an overexpressing strain of *Escherichia coli* pAR1219/Bl12 (Davanloo et al., 1984) according to published methods (Wyatt et al., 1991). After optimizing transcription conditions, a 50 mL transcription reaction yielded 15−20 mg of the desired RNA, which was purified by preparative (42 cm × 45 cm × 0.4 cm, Aquebogue, NY) polyacrylamide (20%) gel electrophoresis. The desired RNA, excised and electroeluted (elutrap, Schleicher & Schuell, Keene, NH) from the gel, was concentrated by ethanol precipitation and exchanged into the desired NMR buffer by centricon filtration (Centricon-3, Amicon, Beverly, MA). Typical transcription conditions are 40 mM Tris (pH 8.0), 1 mM spermidine, 10 mM DTT, 15−20 mM $MgCl_2$, 5 mM GMP, and 20 mM total NTPs, with ~0.1 μM DNA template. The typical NMR buffer is 10 mM sodium phosphate and 0.2 mM EDTA at pH 6.7.

Preparation of Uniformly ^{13}C- and ^{15}N-Labeled AMP and RNA. Uniformly ^{13}C- and ^{15}N-labeled NMPs and NTPs were prepared essentially according to published methods (Nikonowicz et al., 1992). *E. coli* (My285) overexpressing ribosomal RNA (rRNA) were grown in minimal media containing [^{13}C]glucose and [^{15}N]ammonium sulfate as the sole carbon and nitrogen sources. The cells were harvested and ruptured. The rRNA, obtained by phenol extraction, ultracentrifugation, and centrifugation, was enzymatically degraded to nucleoside monophosphates (NMPs). About 200 mg of labeled NMPs was obtained from 2.5 L of cell culture. The labeled NMPs were either separated into individual NMP by ion-exchange chromatography (Mono Q HR 10/10, Pharmacia, Piscataway, NJ) or enzymatically phosphorylated to NTPs. The ion-exchange chromatography was performed at room temperature using 10 mM sodium phosphate at pH 3.4. The labeled AMP was obtained in the second fraction eluted with 1 M NaCl/10 mM sodium phosphate from the Mono Q column. It was then ethanol precipitated, reconstituted, and used for NMR studies. The uniformly labeled RNA aptamer **2** was enzymatically synthesized from labeled NTPs by *in vitro* transcription and purified as described for the preparation of unlabeled RNA.

NMR Spectroscopy. The two- and three-dimensional (2D and 3D) NMR experiments were acquired on a Varian Unity Plus 600 MHz spectrometer except for the proton−phosphorus correlation experiments and HCCNH-TOCSY experiments, which were acquired on a Varian Unity Plus 500 spectrometer. In multidimensional experiments, quadrature detection in indirect dimensions was accomplished using the States−TPPI (Marion et al., 1989) method, while for COSY and NOESY experiments in H_2O the States (States et al., 1982) method was used. For 1D and NOE difference spectra in H_2O buffer, solvent suppression was achieved using a symmetrically shifted shaped pulse (Smallcombe, 1993). For the spectra in D_2O, low power irradiation of the residual HOD resonance by a radio-frequency field of ~50 Hz was applied during the relaxation delay. For all 2D and 3D spectra on the labeled sample, broad-band ^{13}C or ^{15}N GARP (Shaka et al., 1985) decoupling was applied during the acquisition periods where appropriate. One- and two-dimensional spectra were processed using the Varian VNMR program while three-dimensional spectra were processed with the NMRPipe (Delaglio et al., 1995) program and analyzed with the PIPP software (Garret et al., 1991). Residual water was subtracted from the spectra run in H_2O (10% D_2O) buffer by time domain digital filtering. The ^1H and ^{13}C chemical shifts were indirectly referenced (Wishart et al., 1995) to 2,2-dimethyl-2-silapentane-5-sulfonate (DSS), while ^{15}N and ^{31}P were indirectly referenced to ammonia and trimethyl phosphate (TMP), respectively. The ratio of 0.0 ppm frequencies for $^{31}P/^1H$ was measured in this laboratory as $r = 0.404808688$.

The following 2D and 3D NMR spectra were acquired using an AMP-unlabeled RNA sample: 50, 120, and 250 ms mixing time NOESY spectra at 15 °C in D_2O buffer; 150 and 300 ms mixing time NOESY spectra at 10, 20, 25, and 30 °C; 100 and 200 ms mixing time NOESY spectra at 0 and 10 °C in H_2O buffer using the jump and return pulse sequence (Plateau & Gueron, 1982) for solvent suppression; a 2D (^1H,^1H) COSY spectrum at 15 °C; 40 and 80 ms TOCSY experiments at 15 °C with MLEV-17 (Bax & Davis, 1985) as a mixing sequence; ^1H,^{31}P correlation experiments at 15 and 20 °C (Sklenar et al., 1986); ^1H,^{31}P hetero-TOCSY experiments (Kellogg & Schweitzer, 1993) with 24, 40, 50, 60, and 70 ms mixing time at 15 °C using the DIPSI-2 (Shaka et al., 1988) isotropic mixing sequence.

An uniformly ^{13}C- and ^{15}N-labeled RNA sample complexed with unlabeled AMP was used to acquire the following spectra: 2D (^1H,^{13}C) constant-time HSQC spectra at 10 and 30 °C (Santoro & King, 1992; Vuister & Bax,

1992) with evolution periods optimized for J_{HC} = 200 Hz and the constant-time period set to 28 ms; a sensitivity-enhanced gradient (^{1}H,^{15}N) HSQC (Kay et al., 1992) with the evolution periods optimized for J_{HN} = 85 Hz run on the sample in H_2O (10% D_2O) buffer; 120 ms mixing time at 30 °C and 350 ms mixing time 3D NOESY-HMQC (Zuiderweg et al., 1990) spectra at 10 and 30 °C optimized for J_{CH} = 200 Hz; a 3D HCCH-COSY spectrum at 30 °C (Bax et al., 1990) with the evolution intervals corresponding to J_{HC} = 145 Hz and J_{CC} = 40 Hz; a 3D HCCH-TOCSY spectrum at 30 °C (Clore et al., 1990; Fesik et al., 1990) which employed delays optimized for J_{HC} = 145 Hz and J_{CC} = 40 Hz. A DIPSI-3 mixing scheme (Shaka et al., 1988) was applied during the 15 ms ^{13}C TOCSY spin-lock period at the power of 7.1 kHz. A 2D (^{1}H,^{1}H) version of the HCCH-TOCSY experiment was used to correlate adenine H2 and H8 protons. In this case, the spin-lock time was 65 ms at the power of 3.4 kHz, and the delay for the evolution of the proton−carbon magnetization was set to correspond to J_{HC} = 220 Hz. 2D (^{1}H,^{13}C) and 2D (^{1}H,^{15}N) HMQC-NOESY (Fesik & Zuiderweg, 1988) experiments were run at 0 °C in H_2O (10% D_2O) buffer. In both cases, the mixing time was 150 ms, and the jump and return method was used for water suppression. The delays employed were optimized for J_{HC} = 200 Hz and J_{HN} = 100 Hz. In the 2D (^{1}H,^{1}H) and 2D (^{1}H,^{13}C) HCCNH-TOCSY experiment (Fiala et al., 1996), the proton−carbon and proton−nitrogen delays were set corresponding to coupling constants J_{HC} = 220 and J_{HN} = 90 Hz, the carbon−nitrogen evolution period was set to 13 ms, and the DIPSI-3 mixing scheme (Shaka et al., 1988) was applied during the 55 ms ^{13}C TOCSY spin-lock period at the power of 3.0 kHz. A temperature of 10 °C was found to be optimal for observing the H1-H8/C8 correlations.

The following experiments were acquired for the unlabeled RNA aptamer complexed with uniformly ^{13}C,^{15}N-labeled AMP: 2D (^{1}H,^{13}C) constant-time HSQC spectra at 30 °C with evolution periods optimized for J_{HC} = 200 Hz and the constant-time period set to 28 ms in D_2O; a sensitivity-enhanced gradient (^{1}H,^{15}N) HSQC with the evolution periods optimized for J_{HN} = 85 Hz run on a sample in H_2O (10% D_2O) buffer; a 350 ms mixing time 3D NOESY-HMQC spectrum at 30 °C optimized for J_{CH} = 200 Hz; a 2D version of the HCCH-COSY experiment at 30 °C (Bax et al., 1990) with the evolution intervals corresponding to J_{HC} = 145 Hz and J_{CC} = 40 Hz; a 2D version of the HCCH-TOCSY spectrum at 30 °C which employed delays optimized for J_{HC} = 145 Hz and J_{CC} = 40 Hz in D_2O; 2D (^{1}H,^{13}C) and 2D (^{1}H,^{15}N) HMQC-NOESY experiments run at 150 ms mixing and 0 °C, in H_2O (10% D_2O) buffer. Similarly, the jump and return method was used for water suppression, and the delays employed were optimized for J_{HC} = 200 Hz and J_{HN} = 100 Hz.

The acquisition parameters for two-, three-, and four-dimensional NMR experiments on the AMP−RNA aptamer complex are listed in Supporting Information, Table S1.

RESULTS

AMP−RNA Aptamer Complex Formation. Complex formation has been monitored by recording imino proton spectra of the RNA aptamer **2** on gradual addition of AMP in H_2O buffer (10 mM phosphate, 0.2 mM EDTA), pH 6.7 at 0 °C. The exchangeable proton spectra (8.8−14.8 ppm) of free RNA aptamer **2** and its AMP complex (1.2 equiv) are plotted

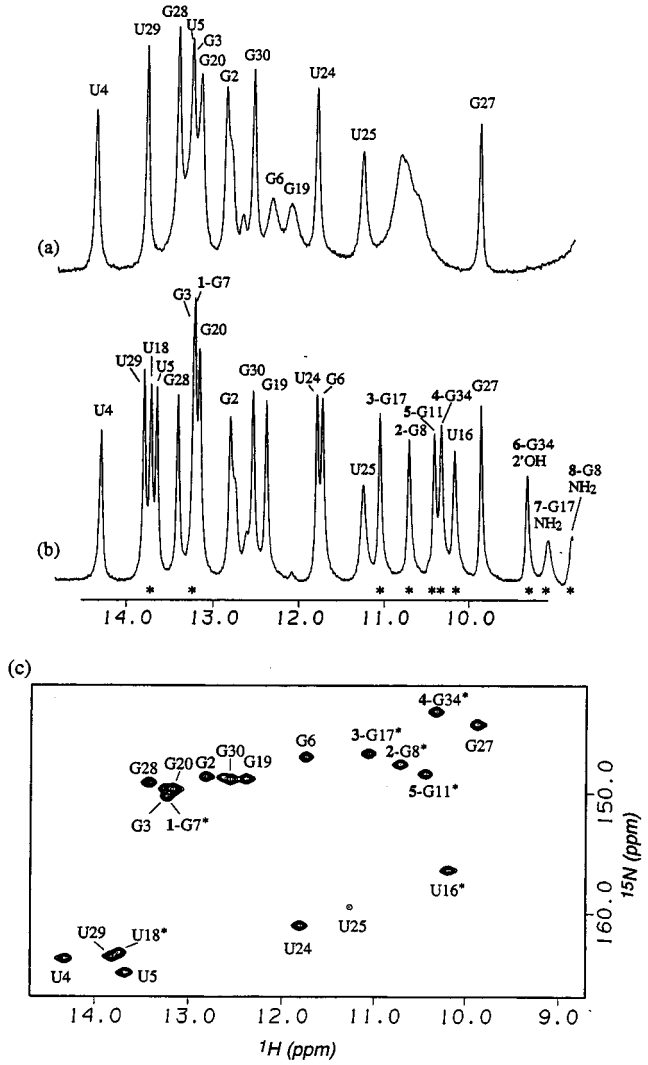

FIGURE 1: Imino proton spectra (8.8−14.8 ppm) of (a) the free RNA aptamer and (b) the AMP−RNA complex (~20% excess AMP) and (c) the imino region of the (^{1}H,^{15}N) HSQC spectrum of the uniformly ^{13}C,^{15}N-labeled AMP−RNA aptamer complex (~50% excess) in H_2O buffer (10 mM sodium phosphate and 0.2 mM EDTA) at pH 6.7 and 0 °C. The concentration of unlabeled and labeled RNA aptamer was ~1.7 and 3.5 mM, respectively. The imino proton assignments based on NOESY and (^{1}H,^{15}N) HSQC experiments are shown over the resonances in the one-dimensional proton spectra. The asterisks in (b) and (c) identify those exchangeable resonances which appeared upon the addition of AMP. The additional exchangeable proton resonances of the internal loop and bulge residues on complex formation are designated by numbers in bold face.

in panels a and b of Figure 1, respectively. Imino proton resonances from both free RNA aptamer and its AMP complex are observed at substoichiometric additions of AMP consistent with slow exchange between free and bound forms. Our studies on the AMP−RNA aptamer complex were undertaken in the presence of a small excess of AMP to ensure complete complex formation.

The imino protons in the spectrum of the free RNA aptamer **2** (Figure 1a) have been assigned on the basis of an analysis of NOESY data sets using standard assignment strategies reported in the literature (Boelens et al., 1985; Patel et al., 1987). The imino protons in the stem segments of free RNA aptamer **2** can be assigned except for the terminal G1 and U18 residues, which have broadened out due to rapid exchange. The imino protons in the internal loop and bulge have also broadened out due to rapid exchange in contrast

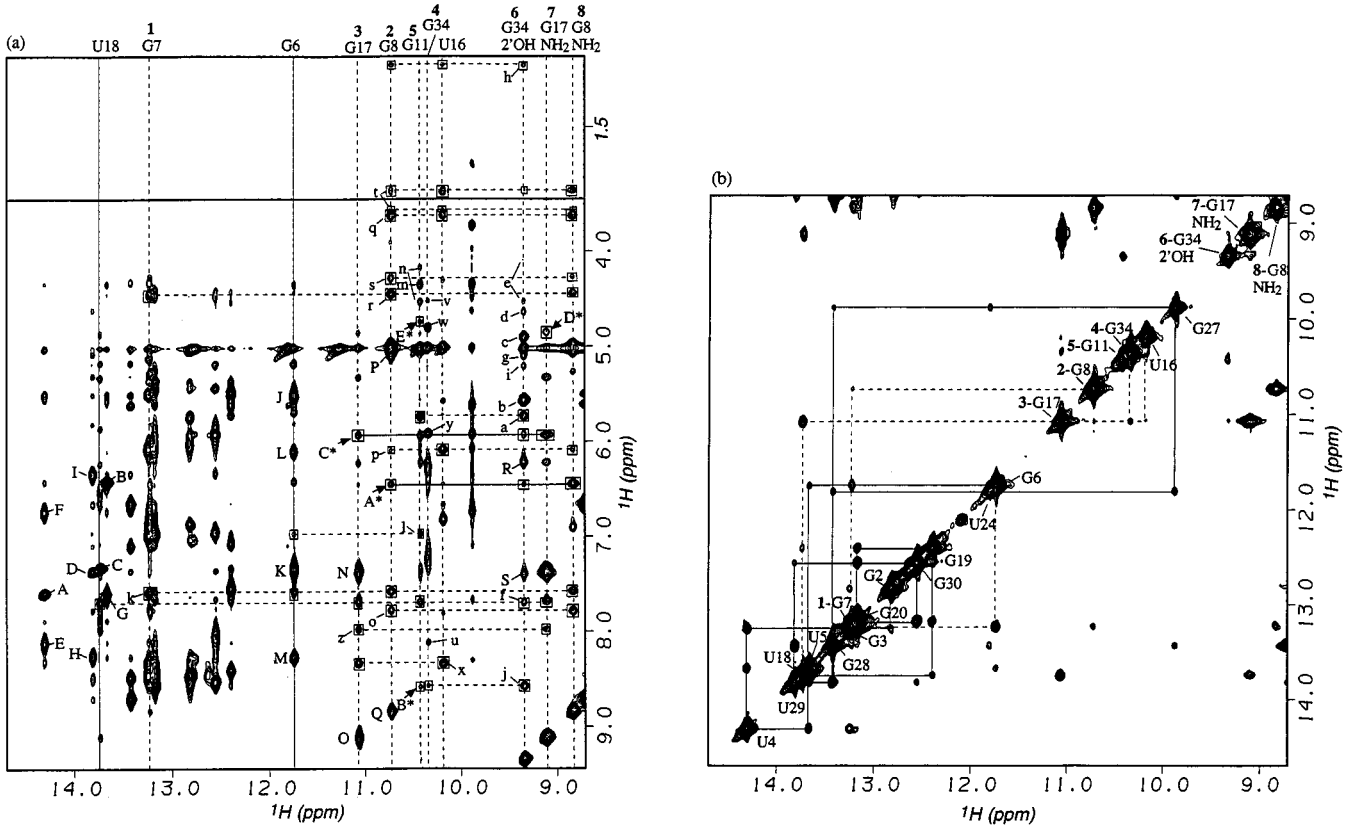

FIGURE 2: Expanded contour plots of (a) the imino (8.8−14.8 ppm) to the base, amino, and sugar proton (3.5−9.5 ppm and 1.5−3.0 ppm) regions and (b) the symmetric imino to imino proton region (8.8−14.8 ppm) of the NOESY (100 ms mixing time) spectra of the AMP−RNA aptamer complex (20% excess AMP) in H_2O buffer, pH 6.7 at 0 °C. The concentration of the RNA aptamer was ∼1.7 mM. (a) The NOE cross peaks from uridine imino protons to adenine H2 and amino protons are labeled as follows: A, U4(NH3)−A37(H2); B, U5(NH3)−A36(H2); C, U18(NH3)−A33(H2); D, U29(NH3)−A22(H2); E, F, U4(NH3)−A37(NH_2); G, U5(NH3)−A36(NH_2) [the other amino proton overlaps with A36(H2)]; H, I, U29(NH3)−A22(NH_2). The cross peaks J to S are assigned as follows: J, K, G6(NH1)−G6(NH_2); L, M, G6(NH1)−C35(NH_2); N, O, **3**-G17(NH1)−G17(NH_2); P, Q, **2**-G8(NH1)−G8(NH_2); R, S, **6**-G34(2′-OH)−A12(NH_2). NOE cross peaks between nonexchangeable and exchangeable protons of RNA are as follows: a, b, c, d, e, f, G34(H1′, H2′, H3′, H4′, H5′/H5″, H8) to **6**-G34(2′-OH); g, h, G11(H1′, H4′) to **6**-G34(2′-OH); i, j, A12(H1′, H8) to **6**-G34(2′-OH); k, G11(H8) to **1**-G17(NH1); l, C35(H6) to **5**-G11(NH1); m, n, C35(H4′, H5′/H5″) to **5**-G11(NH1); o, p, q, r, A10(H8, H1′, H2′, H4′) to **2**-G8(NH1); s, t, G11(H3′, H5′/H5″) to **2**-G8(NH1); u, v, w, A33(H8, H2′, H3′) to **4**-G34(NH1); x, A12(H2) to U16(NH3); y, A12(H1′) to **4**-G34(NH1); z, A10(H8) to **3**-G17(NH1). Dashed horizontal lines from the above cross peaks designate the chemical shifts of respective protons, and NOEs along these lines are identified by boxes. Solid horizontal lines indicate sugar and base protons of AMP which are labeled as follows: A*, AMP(H2); B*, AMP(H8); C*, AMP(H1′); D*, AMP(H2′,H3′); E*, AMP(H4′). NOE cross peaks between AMP and RNA identified in a two-dimensional version of the (^{1}H,^{13}C) HMQC-NOESY experiment with uniformly ^{13}C,^{15}N-labeled AMP complexed with unlabeled RNA aptamer are identified with boxes and connected by horizontal solid lines. (b) The imino proton assignments are labeled along the diagonal. The solid lines trace the NOE connectivities between imino protons on adjacent base pairs along the two stems starting from either G2 at one end or G27/U24 at the other end of the stems and proceeding toward the internal loop. The dashed lines trace the NOE connectivities observed among imino proton resonances within the internal loop and the hairpin bulge.

to the U24, U25, and G27 imino protons in the stable UUCG hairpin loop (Figure 1a).

The exchangeable proton spectrum of the AMP−RNA aptamer **2** complex is simply striking regarding both the narrow line widths and exceptional resolution of the resonances (Figure 1b). Ten new exchangeable protons (labeled by asterisks) can be identified in the well-resolved spectrum of the AMP−RNA aptamer complex in Figure 1b. Two of these resonate between 13.2 and 13.8 ppm, five resonate between 10.2 and 11.2 ppm, and three resonate between 8.8 and 9.3 ppm (Figure 1b). These additional exchangeable resonances must originate from the exchangeable protons of the internal loop and bulge residues together with the flanking U18·A33 stem base pair in the complex. The assignment of these additional exchangeable protons to specific imino and amino protons and sugar hydroxyl protons represented a challenge requiring new approaches to exchangeable proton resonance assignments in non-base-paired segments of RNA.

Stem Imino Proton Assignments. The exchangeable protons in the AMP−RNA aptamer complex spectrum have been subdivided into two categories. Those that originate in the stem regions and the UUCG hairpin loop are labeled by residue position while those in the internal loop and bulge are also labeled by numbers (Figure 1b). The guanine and uracil imino protons that resonate between 9.8 and 14.4 ppm in the complex can be distinguished on the basis of their distinct ^{15}N chemical shifts in (^{1}H,^{15}N) HSQC spectra of the complex containing uniformly ^{13}C,^{15}N-labeled RNA aptamer as shown in Figure 1c.

The imino protons in the two stem segments can be assigned on the basis of NOEs observed in expanded NOESY (mixing time 100 ms) spectra of the complex in H_2O buffer at 0 °C (Figure 2). These include NOEs between uracil imino protons and adenine H2 and amino protons across Watson−Crick A·U base pairs (Figure 2a), between guanine imino protons and cytosine amino and H5 (the latter through spin diffusion) protons across Watson−Crick G·C base pairs (Figure 2a), and between imino protons on adjacent base pairs (Figure 2b). Similarly, a strong NOE between U24 and G27 established formation of a G·U pair in the UUCG

hairpin loop (Figure 2b). These imino proton assignments are listed over the spectrum in Figure 1b and the NOEs relevant to the assignment protocol identified in the caption to Figure 2.

The internal G7 to G17 loop and bulge G34 residues are flanked by the stem G6·C35 and U18·A33 base pairs in the secondary structure of RNA aptamer **2**. The imino proton of G6 is broad in the free RNA aptamer (Figure 1a) but sharpens and shifts upfield to 11.74 ppm on complex formation (Figure 1b). The imino proton of U18 has broadened out in the free RNA aptamer (Figure 1a) but is detected as a narrow resonance at 13.75 ppm in the complex (Figure 1b). The imino proton of G19 of the G19·C32 base pair (which flanks the U18·A33 base pair) is broad in the free RNA aptamer (Figure 1a) but sharpens up and shifts downfield on complex formation (Figure 1b). Overall, the stem imino protons of U5, G6, U18, and G19 of the RNA aptamer shift on AMP complex formation while the remaining stem imino protons that are positioned further away from the internal loop and bulge remain essentially unchanged on complex formation (see Supporting Information tables). In addition, there is a significant slowing down in the complex of the hydrogen exchange characteristics of the imino protons of the stem base pairs (G6·C35, U18·A33, and G19·C32) that flank the internal loop and bulge of the RNA aptamer, resulting in narrow line widths for these resonances on complex formation (Figure 1b).

Stem Amino Proton Assignments. We detect distinctly different patterns for the exocyclic amino protons of the purine rings of the G6·C35 and U18·A33 base pairs that flank the internal loop and bulge residues in the AMP−RNA aptamer complex. The G6 imino proton exhibits strong NOEs to its own resolved amino protons at 5.51 and 7.34 ppm (peaks J and K, Figure 2a) in addition to NOEs to the amino protons of C35 (peaks L and M, Figure 2a) across the base pair in the complex. The imino proton of U18 exhibits a strong NOE to the H2 proton across the U18·A33 base pair in the complex (peak C, Figure 2a). By contrast, we are unable to definitively identify the expected NOEs between the U18 imino proton and the resolved amino protons of A33 in the complex (Figure 2a). This contrasts with the strong uracil imino proton to resolved adenine amino proton NOE patterns observed for other stem U·A base pairs in the complex (Figure 2a).

Internal Loop and Bulge Imino Proton Assignments. We next turn attention to the assignment of the seven imino protons between 10.0 and 14.0 ppm and the three exchangeable protons between 8.8 and 9.5 ppm (designated by asterisks in Figure 1b) that are detected on formation of the AMP−RNA aptamer complex. The most downfield imino proton of the former group (13.75 ppm) has already been assigned to the imino proton of U18 on the basis of its NOE to the imino proton of G19 in the complex. The (^{1}H,^{15}N) HSQC experiment on the complex readily identifies the imino proton at 11.20 ppm to originate in a uracil on the basis of its distinct ^{15}N chemical shift (Figure 1c) and hence is assigned to U16, the only uracil in the internal loop and bulge of the RNA aptamer in the complex. The remaining five imino protons (labeled **1**, **2**, **3**, **4**, and **5**) must originate in the five internal loop and bulge guanines on the basis of their ^{15}N chemical shifts in the (^{1}H,^{15}N) HSQC spectrum of the complex (Figure 1c). One of these guanine imino protons, labeled **1**, resonates at 13.24 ppm in the hydrogen-bonded region while the other four, labeled **2**, **3**, **4** and **5**, resonate further upfield between 10.2 and 11.1 ppm (Figure 1b). The majority of these guanine imino protons exhibit NOEs to one another (Figure 2b) and, in addition, extensive NOEs to base and sugar protons (Figure 2a) in the complex. Thus, the downfield-shifted hydrogen-bonded guanine imino proton resonance **1** (13.24 ppm) exhibits an NOE to the imino proton of G6 of the left helical stem and a weak NOE to the guanine imino proton (10.73 ppm) labeled **2**, suggesting that the base pairing extends from the left stem into the internal loop and bulge segment on complex formation. The guanine imino proton (11.07 ppm) labeled **3** exhibits an NOE to the imino proton of U18 and two weak NOEs to the imino protons of U16 and the guanine imino proton (10.33 ppm) labeled **4**, suggesting that the base pairing also extends from the right stem into the internal loop and bulge segment on complex formation. The guanine imino proton (10.41 ppm) labeled **5** broadens significantly on raising the temperature from 0 °C (Figure 1b) to 25 °C while the guanine imino protons labeled **1**, **2**, **3**, and **4** can be readily detected in the proton spectrum of the complex at 25 °C.

We describe below a new approach recently reported from our laboratory (Fiala et al., 1996) and other laboratories (Sklenar et al., 1996; Simorre et al., 1996) that permits through-bond correlations from the imino proton to independently assigned nonexchangeable H8 proton and C8 carbon positions within individual guanine rings in the complex. The through-bond correlations of guanine imino NH1 protons with their own H8 protons and C8 carbons in HCCNH-TOCSY experiments on the uniformly ^{13}C,^{15}N-labeled RNA aptamer complexed to AMP in H_2O buffer at 10 °C are plotted in panels a and b of Figure 3, respectively. The pulse sequence for this HCCNH-TOCSY experiment as applied to RNA systems has been reported recently from our laboratory (Fiala et al., 1996). These correlations can be detected clearly for the nonterminal G2, G3, G6, G19, G20, G28, and G30 guanines in the stem segment and G27 in the hairpin loop segment of the complex as shown in Figure 3. The imino proton resonances of these eight guanines, assigned from sequential imino−imino NOE connectivities (Figure 2b), correlate well with both H8 and C8 resonances, assigned independently from through-space and through-bond correlations detected for the complex in D_2O solution (see below). These conclusions testify to the robustness of the HCCNH-TOCSY correlation experiments for connecting imino protons with nonexchangeable protons/carbons within individual guanines up to the 40-mer RNA level.

The corresponding imino proton to their own H8/C8 HCCNH-TOCSY correlations for the guanine imino protons labeled **1**, **2**, **3**, **4**, and **5** arising from the internal loop and bulge guanines in the AMP−RNA aptamer complex can be monitored in Figure 3. A knowledge of the guanine H8/C8 assignments of these residues from analysis of NOESY and NOESY-HMQC data sets on the complex in D_2O solution (see below) permits the assignment of imino protons labeled **1**, **2**, **3**, **4**, and **5** to G7, G8, G17, G34, and G11, respectively, in the AMP−RNA aptamer complex (Figure 3). It should be noted that the H8 proton chemical shifts of G17 (labeled **3**) and G34 (labeled **4**) are similar (Figure 3a), as are the C8 carbon chemical shifts of G8 (labeled **2**) and G17 (labeled **3**) (Figure 3b) but that these correlations can be distinguished because the corresponding C8 and H8 chemical shifts are very different in the complex. We recommend that the HCCNH-TOCSY correlations for RNA imino proton as-

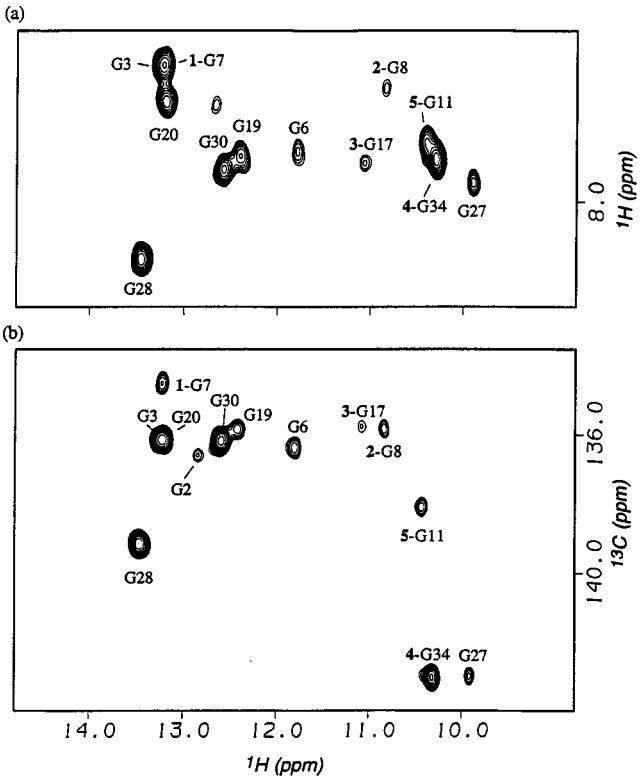

FIGURE 3: Expanded contour plots of HCCNH-TOCSY experiments on the uniformly ^{13}C,^{15}N-labeled RNA aptamer complexed with unlabeled AMP (50% excess) in H_2O buffer, pH 6.7 at 10 °C. The experiments were optimized for the imino proton region and correlate the guanine imino protons with (a) their H8 protons and (b) their C8 carbons. The NH1−C8 and NH1−H8 correlations are observed for all the guanines with the exception of G1. A NH1−C8 correlation cross peak is seen for G2 in (b). A NH1−H8 cross peak corresponding to G2 can be observed on lowering the contour level in (a).

signments be undertaken between the guanine imino protons to both their H8 and C8 positions to resolve ambiguities that could arise due to chemical shift degeneracies.

These internal loop and bulge guanine imino proton assignments in the AMP−RNA aptamer complex have been independently confirmed by one at a time replacement of the G7, G8, G11, G17, and G34 guanines by their ^{15}N-N1,-N2-labeled counterparts on the one hand and by inosine on the other (Jiang et al., 1996b). In the former case, the imino proton of the labeled guanine is clearly identified in the (^{1}H,^{15}N) HSQC experiment, while in the latter case, the imino proton shifts downfield by ∼2 ppm on substituting guanine by inosine. These extensive efforts to unambiguously assign the imino protons of the internal loop and bulge guanines were absolutely necessary since these imino protons exhibit a large number of NOEs to other RNA protons and to bound AMP that turned out to be critical in our efforts at structure determination of the AMP−RNA aptamer complex.

The imino proton and nitrogen chemical shifts in the free and AMP-bound RNA aptamer **2** are listed in Supporting Information, Table S2.

Internal Loop and Bulge Amino Proton Assignments. The exchangeable protons labeled **7** and **8** (Figure 1b) can be assigned to the downfield-shifted hydrogen-bonded amino protons of internal bulge guanines in the AMP−RNA aptamer complex. The G17 imino proton (labeled **3**) at 11.06 ppm exhibits strong NOEs to amino protons at 7.40 and 9.12 ppm in the NOESY spectrum of the AMP−RNA aptamer complex (peaks N and O along the vertical dashed line for **3**, Figure 2a). This permits the assignment of the 9.12 ppm exchangeable proton resonance (labeled **7**) to the G17 amino proton which must be hydrogen bonded due to its unusually downfield shift in the spectrum. The G8 imino proton (labeled **2**) at 10.72 ppm exhibits strong NOEs to amino protons at 5.03 and 8.84 ppm in the NOESY spectrum of the AMP−RNA aptamer complex (peaks P and Q along the vertical dashed line for **2**, Figure 2a). This permits the assignment of the 8.84 ppm exchangeable proton resonance (labeled **8**) to the G8 amino proton which must be hydrogen bonded due to its downfield shift in the spectrum. The G8 and G17 amino proton assignments have been independently established from studies of selective incorporation of ^{15}N-N1,N2-guanines at positions 8 and 17 in the AMP−RNA aptamer complex (Jiang et al., 1996b). It should be noted that the N2 nitrogen chemical shift for G8 (76.6 ppm) in the complex falls within the range typically observed for guanine N2 amino nitrogens while that for G17 (82.2 ppm) in the complex is further downfield and approaches values typically observed for adenine N6 amino nitrogens (Supporting Information, Figure S1).

One set of resolved adenine amino protons has been identified in addition to those participating in Watson−Crick base pair formation in the two stems of the AMP−RNA aptamer complex. This adenine amino proton pair at 6.21 and 7.40 ppm has been assigned to A12 on the basis of through-bond correlations in HCCNH-TOCSY experiments to the independently assigned H2 and H8 protons of A12 (based on the observation of three of the four expected correlation cross peaks) in the complex. This adenine amino proton assignment has been independently established also from studies of selective incorporation of ^{15}N-N6-adenine at position 12 in the AMP−RNA aptamer complex (Jiang et al., 1996b).

Two cytosine amino proton pairs can be detected in (^{1}H,^{15}N) HSQC experiments in addition to those participating in Watson−Crick base pair formation in the two stems of the AMP−RNA aptamer complex. One cytosine amino proton pair (6.37 and 7.11 ppm) has been assigned to C26 in the UUCG hairpin loop in the complex because both proton and nitrogen chemical shifts of this amino group are not affected by AMP binding. The other cytosine amino proton pair (6.62 and 7.09 ppm) with a ^{15}N chemical shift of 97.4 ppm is assigned by elimination to the C15 residue in the internal loop of the complex. The small chemical shift difference between the amino protons of C15 ($\Delta\delta = 0.47$ ppm) suggests that these amino protons do not likely participate in hydrogen bond formation in the AMP−RNA aptamer complex.

Sugar Hydroxyl Proton Assignment. The exchangeable proton labeled **6** at 9.34 ppm exhibits a singlet pattern in the heteronuclear undecoupled proton spectrum of the uniformly ^{13}C,^{15}N-labeled RNA aptamer **2** bound to AMP or of RNA aptamer **2** bound to uniformly ^{13}C,^{15}N-labeled AMP. It therefore cannot be a carbon-linked or nitrogen-linked (imino or amino) proton and must originate in a hydroxyl group. The exchangeable proton labeled **6** exhibits a large number of NOEs to the independently assigned nonexchangeable sugar protons of G34, the strongest being to the H2′ proton of this guanine (peak b, Figure 2a), in the complex. This permits the assignment of the exchangeable proton labeled **6** to the 2′-hydroxyl group of G34 in the AMP-RNA aptamer complex. This 2′-OH assignment also turns out to be a critical one, based on the large number of

NOEs involving the G34 2′-OH proton to other RNA protons and to AMP in the complex (Figure 2a).

It should be noted that the 9.34 ppm chemical shift of the 2′-OH of G34 in the AMP-RNA aptamer complex is downfield of the approximately 6.8 ppm chemical shift for a 2′-OH proton (Allain & Varani, 1995) in the stable UUCG RNA hairpin loop (Cheong et al., 1990). Both the narrow line width and the large downfield shift of the 2′-OH of the G34 residue suggest that the hydroxyl proton is most likely shielded from solvent and participates in hydrogen bond formation in the solution structure of the AMP−RNA aptamer complex.

Stem Nonexchangeable Proton Assignments. The assignment of the nonexchangeable protons in the 40-mer RNA aptamer complexed to AMP has required the application of a range of homonuclear and heteronuclear multidimensional NMR experiments. The strategy that was followed included initial analysis of two-dimensional homonuclear NOESY, COSY, and TOCSY and heteronuclear (^{1}H,^{13}C) HSQC data sets with ambiguities in chain tracing resolved by analysis of heteronuclear (^{1}H,^{31}P) COSY, (^{1}H,^{31}P) TOCSY, and (^{1}H,^{13}C) NOESY-HMQC data sets on the AMP−RNA aptamer complex in D_2O solution.

Initially, the base (purine H8 and pyrimidine H6) protons in the AMP−RNA aptamer complex were differentiated on the basis of their distinct spectral characteristics. Thus, the nine cytosines and four uracils in the two stems could be identified by their characteristic H5−H6 NOE and coupling connectivities, and distinguished by class on the basis of the upfield shifts of the C5 carbons of cytosines relative to uracils. It was possible to distinguish adenine from guanine H8 protons since the former exhibit through-bond connectivities to their adenine H2 protons in (^{1}H,^{13}C) HCCH-TOCSY experiments (Legault et al., 1994; Marino et al., 1994). Further, the stem adenine H2 protons have been independently assigned on the basis of their NOEs to identified uracil imino protons across the Watson−Crick A·U base pairs in the complex.

The sequential base proton to its own and 5′-flanking sugar H1′ proton NOE connectivities within the leftward stem (G1 to G6 and C35 to C40) and the rightward stem (U18 to C23 and G28 to A33) are traced in expanded NOESY (250 ms mixing time) contour plots of the AMP−RNA aptamer complex in D_2O solution at 15 °C in panels a and b of Figure 4, respectively. The tracing is less than straightforward since the base protons of no less than 20 residues resonate between 7.6 and 7.9 ppm with the overlap especially severe centered about 7.67 ppm. The sequential connectivities for the stem segments outlined in Figure 4 are greatly aided by analysis of individual ^{13}C planes in the (^{1}H,^{13}C) NOESY-HMQC data sets of the complex.

The most unusual feature of the base and sugar H1′ protons of the leftward stem is the large upfield shift of the H1′ proton of C35 (5.05 ppm) from the G6·C35 base pair that flanks the internal loop and bulge residues in the complex (Figure 4a). The most unusual feature of the base and sugar H1′ protons of the rightward stem is the unusually large upfield shift of the H1′ proton of G28 from the C23·G28 base pair that closes the stable UUCG hairpin loop. Such an upfield shift has been reported from earlier studies on UUCG hairpin loop−stem structures (Varani et al., 1991). It should also be noted that the NOE between the H6 and H1′ protons of U18 (cross peak labeled U18 in Figure 4b) is unusually weak in the complex most likely due to broadening of one or both of these protons of this uracil in the U18·A33 base pair that flanks the internal loop and bulge in the complex.

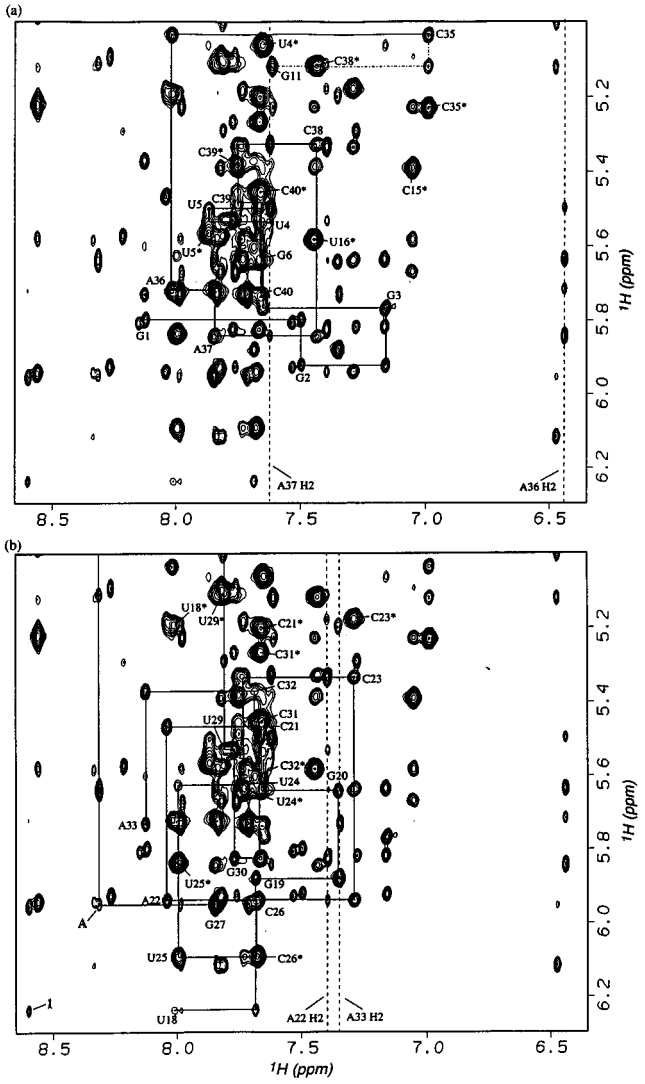

FIGURE 4: Duplicate expanded NOESY (250 ms mixing time) contour plots outlining NOE connectivities between the base proton (6.45−8.65 ppm) and the sugar H1′ proton (5.0−6.3 ppm) regions for the AMP−RNA aptamer complex in D_2O buffer, pH 6.7 at 15 °C. The sequential NOE connectivities between the base proton and their own and 5′-flanking sugar H1′ protons are shown by solid lines in (a) for the left stem from G1 to G6 and from C35 to C40 and in (b) for the right stem and hairpin loop from U18 to A33. The labeled peaks identify the base to their own sugar H1′ NOEs while the cytosine and uracil H6−H5 NOEs are designated by asterisks. Dashed vertical lines designate adenine H2 protons from the two stems. Four NOE cross peaks to sugar H1′ protons were observed as expected for each adenine H2 proton in the helical stems [except that three were observed for A33(H2)]. A very weak NOE is observed between the H6 proton and its own H1′ proton for U18 (labeled U18). The weak sequential NOE between the H8 proton of G27 and the H1′ proton of C26 is labeled **A**. The intermolecular NOE between the H1′ proton of U18 and the H8 proton of AMP is labeled **1**.

An attempt was next made to correlate the H1′ protons with the remaining sugar protons (H2′, H3′, H4′, and H5′,5″) for individual residues in the stem segments through analysis of three-dimensional (^{1}H,^{13}C) HCCH-COSY and (^{1}H,^{13}C) HCCH-TOCSY data sets on the complex in D_2O solution at 30 °C. We were successful in assigning ∼50% of these sugar protons and were precluded from a complete analysis due to severe spectral overlap even in the three-dimensional

Table 1: ^{1}H, ^{13}C, ^{15}N, and ^{31}P Chemical Shifts (ppm) of the Internal Loop (G7 to G17) and Bulge (G34) Residues and Two Closing Base Pair (G6·C35 and U18·A33) Residues of the AMP−RNA Aptamer Complex[a]

base	H8/H6	H2/H5	H1′	H2′	H3′	H4′	H5′,H5″ [d]	NH1/NH3	NH_2
G6	7.68		5.64	4.10	4.80	4.36	4.10, 4.57	11.74	5.51, 7.34
G7	7.20		5.82	4.39	4.57	4.36	4.07, 4.48	13.24	−[e]
G8	7.29		5.30	4.27	4.71	4.27	4.10, 4.39	10.72	5.03, 8.84[b]
A9	8.24	7.84	5.58	4.54	(4.51)[c]	4.24	(4.04, 4.51)[c]		−
A10	7.82	7.99	6.13	3.66	4.99	4.48	3.95, 4.30		−
G11	7.63		5.13	4.45	4.33	1.60	2.98, 3.57	10.41	−
A12	8.55	8.33	5.97	5.21	4.99	4.62	3.75, 4.16		6.21, 7.40
A13	8.25	7.78	5.94	5.09	4.57	4.66	4.33, 4.60		−
A14	7.84	7.99	5.68	4.42	4.68	4.51	4.22, 4.54		−
C15	7.07	5.35	5.24	4.24	4.22	4.30	4.04, 4.39		6.62, 7.09
U16	7.45	5.58	5.58	4.77	4.33	(4.36)[c]	(4.04, 4.30)[c]	10.2	
G17	7.75		5.74	4.36	4.71	4.07	(3.95, 4.27)[c]	11.06	7.40, 9.12
U18	8.02	5.20	6.24	4.86	4.68	4.45	4.14, 4.62	13.75	
A33	8.12	7.36	5.74	4.51	4.80	4.33	(4.01, 4.39)[c]		−
G34	7.73		5.72	5.59	4.92	4.68	4.12, 4.60	10.33	−
C35	6.99	5.27	5.05	4.36	4.36	4.37	4.16, 4.48		6.11, 8.28

base	C8/C6	C2/C5	C1′	C2′	C3′	C4′	C5′	N1/N3	N2/N4/N6	P[f]
G6	136.6		92.2	75.7	72.1	82.0	64.7	147.0	74.0	−
G7	134.7		92.2	75.7	72.1	81.6	64.3	150.3	−	−
G8	135.9		93.9	75.7	71.3	82.3	64.0	147.6	76.6	−3.43
A9	142.6	153.8	94.2	75.0	(71.7)[c]	83.1	(64.4)[c]		−	−
A10	139.7	155.4	93.9	77.6	71.7	83.8	64.4		−	−2.90
G11	138.1		85.3	73.9	78.0	85.7	67.3	148.4	−	−5.25
A12	141.4	157.3	89.8	74.3	79.8	87.5	68.8		86.1	−3.95
A13	141.6	153.9	93.9	75.7	74.6	83.5	68.0		−	−2.32
A14	138.7	154.9	92.4	75.7	72.1	82.4	64.4		−	−
C15	139.4	98.0	93.7	75.7	71.7	81.6	64.0		97.4	−
U16	139.8	104.8	93.3	75.0	72.8	(82.0)[c]	(64.7)[c]	156.4		−
G17	135.8		92.3	76.1	73.2	81.2	(64.0)[c]	146.7	82.2	−
U18	141.8	104.0	93.5	75.7	72.4	81.6	64.0	163.3		−
A33	139.6	154.6	94.0	75.4	72.4	82.4	(65.8)[c]		−	−
G34	143.0		90.5	69.9	78.0	86.4	67.4	143.2	−	−
C35	140.4	98.2	94.3	75.0	73.9	82.0	65.8		97.4	−1.78

[a] NMR spectra were obtained in 10 mM sodium phosphate and 0.2 mM EDTA, pH 6.7, at 0 °C for imino/amino protons and nitrogens, at 30 °C for nonexchangeable protons and carbons, and at 20 °C for phosphorus. Chemical shifts of protons were referenced relative to the H_2O signal (5.01 ppm at 0 °C, 4.71 ppm at 30 °C, and 4.81 ppm at 20 °C) while chemical shifts of nitrogens, carbons and phosphorus were referenced indirectly to ammonia, TSP, and TMP, respectively. Chemical shifts are accurate to ±0.1 ppm for carbons and nitrogens and to ±0.02 ppm for protons and phosphorus. [b] The upfield amino proton of this guanine cannot be seen at 0 °C due to its proximity to the water solvent resonance at this temperature. It can, however, be identified clearly in the spectrum obtained at 10 °C. The chemical shift of 5.03 ppm corresponds to its value at 10 °C. [c] Tentative assignments are parenthesized. [d] The geminal sugar H5′,5″ protons are not stereospecifically assigned. [e] (−) indicates that the resonance either is not observed or cannot be assigned. [f] These are chemical shifts for the phosphorus atoms in the $(n)-P-(n+1)$ steps with the value listed for residue $(n+1)$.

heteronuclear data sets of the complex. The base and sugar nonexchangeable proton chemical shifts of the G6·C35 and U18·A33 base pairs on either side of the internal loop and bulge residues of the ATP−RNA aptamer complex at 30 °C are listed in Table 1 while the corresponding available values for the remaining stem base pairs are listed in Supporting Information, Table S3.

The NOE and sugar coupling constant patterns are consistent with the formation of standard A-form helices with C3′-endo sugar puckers (H1′-H2′ couplings cannot be detected) for the leftward and rightward stem segments in the AMP−RNA aptamer complex. The H2 protons for adenines at positions A36 and A37 (Figure 4a) and at positions A22 and A33 (Figure 4b) in the stem segments exhibit directional NOEs to same strand and cross strand sugar H1′ protons that are also characteristic of A-form helices in solution.

Internal Loop Nonexchangeable Proton Assignments. The base proton−sugar H1′ proton tracing of the 11 residues in the internal loop of the AMP−RNA aptamer complex was greatly facilitated by supplementing the information from the homonuclear NOESY data sets with the corresponding information from three-dimensional (^{1}H,^{13}C) NOESY-HMQC and two-dimensional (^{1}H,^{31}P) COSY data sets on the AMP−RNA aptamer complex in D_2O solution. The base and sugar H1′ assignments were cross-checked with other regions of the homonuclear and heteronuclear multidimensional data sets since there are breaks in the connectivity tracing associated with unusual conformations in the internal loop of the complex. The base proton to its own and 5′-flanking sugar H1′ proton chain tracing from G6 to U18 of the internal loop segment is outlined in strip plots corresponding to individual C1′ chemical shift planes from three-dimensional (^{1}H,^{13}C) NOESY-HMQC data sets on the complex (Figure 5a). The tracing exhibits weak connectivities at the G8−A9 and G11−A12 steps and breaks at the A10−G11 and A12−A13 steps within the internal loop segment of the complex. We were able to independently identify the A10−G11, G11−A12, and A12−A13 connectivities since these steps can be followed in the (^{1}H,^{31}P) COSY correlation experiment on the complex (see below).

The tracing for the G8−A9 step is based on a self-consistent set of NOEs between protons on the G8-A9-A10 segment of the internal loop in the complex. Specifically, the H1′ proton of G8 (5.30 ppm) exhibits weak and strong NOEs, respectively, to the H8 protons of A9 (8.24 ppm) and

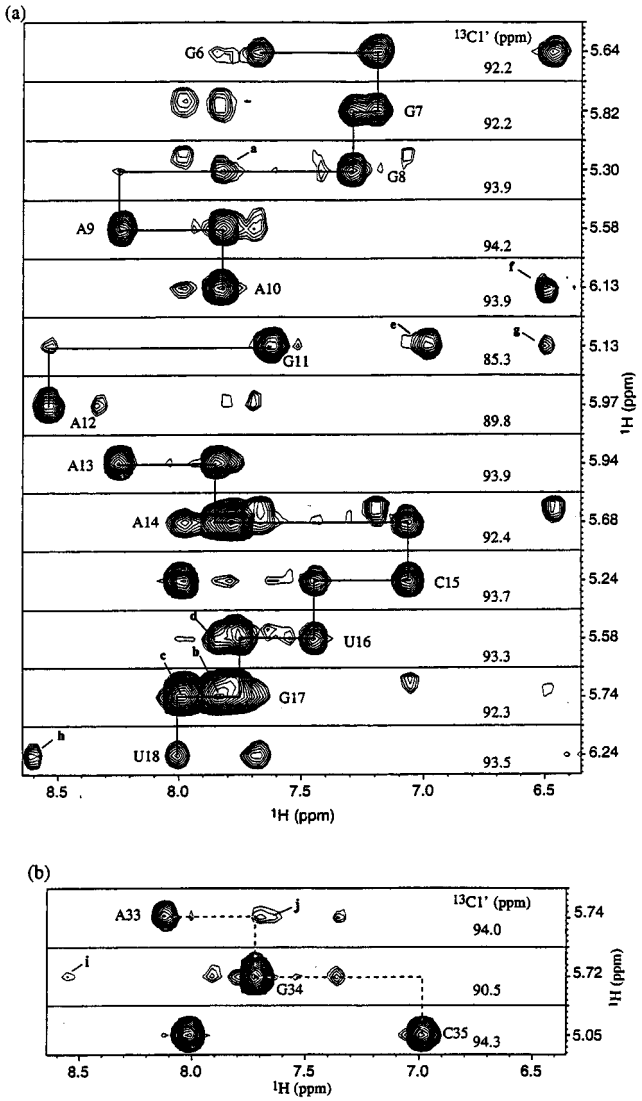

FIGURE 5: Strip plots of (^{1}H,^{13}C) NOESY-HMQC spectra (350 ms mixing time) of the uniformly ^{13}C,^{15}N-labeled RNA aptamer complexed with unlabeled AMP in D_2O buffer, pH 6.7 at 30 °C, showing the aromatic region of H1′ strips at corresponding C1′ planes for (a) the internal loop and (b) the internal bulge. The labeled peaks identify NOEs between the base protons and their own sugar H1′ protons. Solid lines in (a) trace the base proton−sugar H1′ proton walk starting from G6 at the top toward U18 at the bottom which spans the internal loop residues. Note that NOEs from G8(H1′) to A9(H8) and from G11(H1′) to A12(H1′) are very weak and NOEs from A10 H1′ to G11(H8) and A12(H1′) to A13(H8) are completely absent even at a mixing time of 350 ms. Dashed lines in (b) trace NOEs along the base proton−sugar H1′ proton walk from A33 to C35 with NOEs from A33(H1′) to G34-(H8) and G34(H1′) to C35(H6) either very weak or missing. Unusual long-range NOEs in the internal loop and intermolecular NOEs between AMP and RNA are identified as follows: a, G8(H1′)−A10(H8); b, G17(H1′)−A9(H2); c, G17(H1′)−A10(H2); d, U16(H1′)−A9(H2); e, G11(H1′)−C35(H6); f, A10(H1′)−AMP(H2); g, G11(H1′)−AMP(H2); h, U18(H1′)−AMP(H8); i, G34(H1′)−A12(H8), j, the purported position for A33(H1′)−G11(H8).

A10 (7.82 ppm), both of which in turn exhibit an NOE to the H1′ proton of A9 (5.58 ppm). The H8 proton of A10 also exhibits an NOE to its own H1′ proton (6.13 ppm) and a strong long-range NOE (discussed above) to the H1′ proton of G8 (peak a, Figure 5a) in the complex.

The assigned sugar H1′ protons in the internal loop of the complex could be next correlated with the remaining protons within individual sugars following analysis of three-dimensional (^{1}H,^{13}C) HCCH-COSY and (^{1}H,^{13}C) HCCH-TOCSY experiments (Supporting Information, Figures S2 and S3). The base and sugar proton and carbon chemical shifts of the internal loop residues in the AMP−RNA aptamer complex are listed in Table 1. We observe unusual chemical shifts for several internal loop protons in the complex. The H8 proton of A12 (8.55 ppm) resonates downfield while those of G7 (7.20 ppm) and G8 (7.29 ppm) resonate upfield from their unperturbed counterparts in the complex. We also observe unusual upfield shifts at the H2′ proton of A10 (3.66 ppm) and at the H1′ (5.13 ppm), H4′ (1.60 ppm), and H5′,5″ (2.98, 3.57 ppm) protons of G11 while an unusual downfield shift is observed at the H2′ of G34 (5.59 ppm) in the complex (Table 1).

Internal Bulge Nonexchangeable Proton Assignments. The base proton−sugar H1′ proton chain tracing for the G34 internal bulge residue within the AMP−RNA aptamer complex is outlined for the A33-G34-C35 segment in Figure 5b. A33 and C35 are stem residues whose base and sugar protons were assigned as outlined above on the basis of the chain tracing within the stem segments. The G34 bulge residue was distinguished from other internal loop guanines on the basis of through-bond correlations for the G34−C35 step observed in the (^{1}H, ^{31}P) COSY spectrum of the complex (see below). There are breaks in the sequential base proton to sugar H1′ proton connectivities at both A33−G34 and G34−C35 steps in this segment of the complex (Figure 5b). The base and sugar proton chemical shifts of the G34 bulge residue in the complex are listed in Table 1.

Sequential Connectivities Based on Proton−Phosphorus Correlations. The proton-decoupled phosphorus spectrum of the AMP−RNA aptamer complex is plotted in Figure 6a. Several resonances are observed to low and high field of the main cluster of phosphorus resonances dispersed between −3.8 and −4.6 ppm upfield from standard trimethyl phosphate. The phosphorus assignments are based on through-bond correlations to the H3′ proton in the 5′-direction and the H4′ and/or H5′,5″ protons in the 3′-direction following analysis of the (^{1}H,^{31}P) COSY (Figure 6b) and (^{1}H,^{31}P) TOCSY data sets on the complex in D_2O solution. These connectivities are observed for the phosphates at the G7−G8 (−3.43 ppm), A9−A10 (−2.90 ppm), A10−G11 (−5.25 ppm), G11−A12 (−3.95 ppm), and A12−A13 (−2.32 ppm) steps in the internal loop segment and the G34−C35 (−1.78 ppm) step in the internal bulge segment of the complex (Figure 6b). The phosphates at the U25−C26 (−5.17 ppm), C26−G27 (−5.06 ppm), and G28−U29 (−4.84 ppm) steps in the UUCG hairpin loop resonate to high field of the main phosphate cluster in the complex (Figure 6b). The chemical shifts of the assigned phosphorus resonances in the AMP−RNA aptamer complex are listed in Table 1 and Supporting Information, Table S3.

Sugar Pucker Geometrics. The C3′-endo and C2′-endo families of sugar pucker geometries for the 40 residues in the AMP−RNA aptamer complex can be distinguished on the basis of the magnitude of the *J*(H1′,H2′) coupling constants since a negligible coupling is predicted for the former sugar pucker and a large coupling is predicted for the latter sugar pucker. We observe distinct *J*(H1′,H2′) coupling cross peaks for the internal loop G11 and A12 residues, the internal bulge G34 residue, the hairpin loop U25 and C26 residues, and the 3′-terminal C40 residue in the COSY spectrum of the complex (Supporting Information, Figure S4). A comparative analysis of the experimental COSY contour patterns with their simulated counterparts

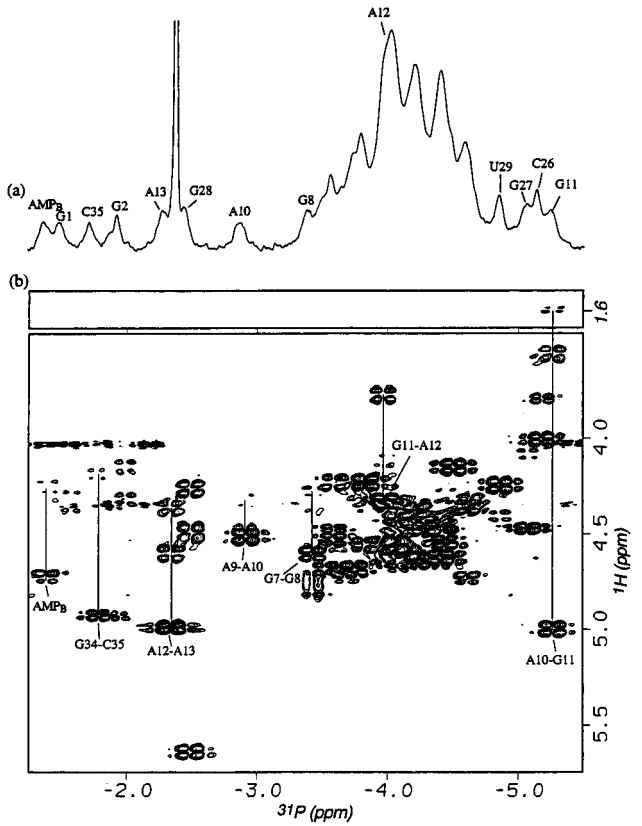

FIGURE 6: (a) One-dimensional proton-decoupled phosphorus spectrum (15 °C) and (b) expanded contour plot of the proton-detected phosphorus−proton heteronuclear correlation experiment (20 °C) for the AMP−RNA aptamer complex in D_2O buffer at pH 6.7. Phosphorus chemical shifts are referenced to an external TMP standard. The assignments for outlying phosphorus resonances are shown in (a). The narrow off-scale phosphorus resonance (at −2.38 ppm) is from phosphate buffer. The correlation cross peaks between phosphorus and its 5′-flanking sugar H3′ protons are labeled in (b) for steps where sequential NOE connectivities in the NOESY spectrum were either very weak or missing.

yields *J*(H1′,H2′) coupling constants of 9.5, 7.8, and 9.0 Hz and *J*(H2′,H3′) coupling constants of 5.0, 5.8, and 5.6 Hz for G11, A12, and G34 residues, respectively, in the complex. These coupling constants confirm the predominant formation of C2′-endo pucker at the internal loop G11 and A12 residues and internal bulge G34 residue in the AMP−RNA aptamer complex.

Glycosidic Torsion Angles. The anti and syn families of glycosidic torsion angles for the 40 residues in the AMP−RNA aptamer complex can be distinguished on the basis of the magnitude of the NOE between the base (purine H8 or pyrimidine H6) proton and its own sugar H1′ proton since a weak NOE is predicted for the anti (∼3.7 Å separation) and a strong NOE is predicted for the syn (∼2.5 Å separation) glycosidic torsion angle alignment (Patel et al., 1982). We observe strong NOEs between the base and their own sugar H1′ protons for the hairpin loop G27 residue and the internal bulge G34 residue in short (50 ms) mixing time NOESY data sets on the AMP−RNA aptamer complex with intensities comparable to the NOEs between the H5 and H6 protons of cytosine (fixed distance of 2.45 Å) residues. Consistent with this observation, the chemical shift of the H2′ proton of G34 (5.59 ppm) and the chemical shift of the H3′ proton of G27 (5.62 ppm) are shifted downfield, reflecting in-plane ring current contributions associated with the syn alignment of purine bases and the respective C2′-endo and C3′-endo puckers of the two guanines in the complex.

Our observation of a syn glycosidic torsion angle at G27 in the U24-U25-C26-G27 hairpin loop in the complex is consistent with the earlier establishment of syn glycosidic torsion angles for the guanine residue in UUCG hairpin loops (Variani et al., 1991). The syn glycosidic torsion angle at the G34 internal bulge residue was unexpected and provides a unique alignment for this residue which is critical for both the topology of the internal bulge and the generation of the AMP binding pocket.

Sugar Carbon Chemical Shifts. Recent studies have noted that the sugar C1′, C3′, and C4′ carbons exhibit distinct chemical shifts for C2′-endo and C3′-endo sugar puckers for residues with anti glycosidic torsion angles (Ghose et al., 1994; Greene et al., 1995). Thus, the C1′ carbons resonate at ∼86 ppm for C2′-endo sugar puckers and are shifted by up to 7 ppm downfield for C3′-endo puckers. By contrast, C3′ carbons resonate at ∼78 ppm and C4′ carbons resonate at ∼86 ppm for C2′-endo sugar puckers with both shifting upfield by ∼5 ppm for C3′-endo sugar puckers (Greene et al., 1995; Greenbaum et al., 1995; Fan et al., 1996).

The G11 residue exhibits C1′, C3′, and C4′ carbon chemical shifts of 85.3, 78.0, and 86.4 ppm, respectively (Table 1), consistent with a C2′-endo pucker geometry in the AMP−RNA aptamer complex. Similarly, the C3′ and C4′ carbon chemical shifts of 79.8 and 87.5 ppm for A12 and the corresponding shifts of 78.0 and 86.4 ppm for G34 (Table 1) are consistent with C2′-endo pucker geometries for these residues in the complex. The C1′ chemical shifts of 89.8 and 90.5 ppm for A12 and G34, respectively (Table 1), in the complex are downfield of the C2′-endo pucker range. The downfield shift for the C1′ carbon of G34 must originate in the syn glycosidic torsion angle for this residue in the complex since it has been previously shown that downfield shifts ranging from 3 to 5 ppm are observed for C1′ carbons that adopt syn glycosidic torsion angles (Wang et al., 1991; Mao et al., 1995).

Unusual Sequential and Long-Range NOEs within the Internal Loop and Bulge. The assignment of the exchangeable imino and amino protons and nonexchangeable base and sugar protons of the internal loop (G7 to G17) and bulge (G34) residues together with their flanking base pairs (G6·C35 and U18·A33) permits the identification of unusual sequential and long-range NOEs within this segment of the AMP−RNA aptamer complex. These NOEs are summarized in Table 2 and provide important restraints for structural characterization of features of the internal loop and bulge segments of the AMP−RNA aptamer complex.

The G7-G8-A9-A10-G11 Segment. There are several unusual NOEs within the G7-G8-A9-A10-G11 segment which are suggestive of a hairpin-like chain reversal by the G8-A9-A10 segment closed by a G7·G11 mismatched pair. The extremely weak sequential connectivities between G8 and A9 suggest that the chain reversal must occur at this step. The key NOEs are made by the imino and amino protons of G8 to the base and sugar protons of A10 (strongest NOEs to the H2′ and H3′ protons) and G11 (strongest NOE to the H8 proton) (Table 2 and Figure 2a), suggesting that the Watson−Crick edge of G8 be directed toward and between the sugar−phosphate backbone of the A10−G11 step. The absence of sequential NOEs between A10 and G11 together with the C2′-endo sugar pucker at G11 implies an extended backbone at the A10−G11 step. In addition, sequential NOEs are observed between adjacent G6 and G7 residues (Table 2) and between nonadjacent G11 and C35

Table 2: Unusual Sequential and Long-Range (between Nonadjacent Residues) NOEs between RNA Residues in the AMP−RNA Aptamer Complex[a]

proton	NOEs
G6	
NH-1	G7 (NH-1), G11 (H8)
G7	
NH-1	G6 (NH-1), G8 (NH-1), G11 (H8, H2′)
G8	
NH-1	A10 (H8, H1′, H2′, H3′, H4′, H5′/H5″), G11 (H8, H2′, H3′, H4′, H5′/H5″)
NH_2-2	A10 (H8, H1′, H2′, H3′), G11 (H8, H2′, H3′, H5′/H5″)
H1′	A10 (H8)
A9	
H2	U16 (NH-3, H1′), G17 (H8, H1′, H2′, H3′, H4′, H5′/H5″)
A10	
H2	G17 (NH-1, NH_2-2, H8, H1′, H2′, H3′)
H8	G8 (NH-1, NH_2-2, H1′)
H1′	G8 (NH-1, NH_2-2), U16 (NH-3), G17 (H1′)
H2′, H3′	G8 (NH-1, NH_2-2), U16 (NH-3)
H4′, H5′/H5″	G8 (NH-1)
G11	
NH-1	G34 (H8, H1′), C35 (H6, H1′, H4′, H5′/H5″)
H8	G6 (NH-1), G7 (NH-1), G8 (NH-1, NH_2-2), C35 (H5)
H1′	G34 (2′-OH), C35 (H5, H6)
H2′	G7 (NH-1), G8 (NH-1, NH_2-2)
H3′	G8 (NH-1, NH_2-2)
H4′	G8 (NH-1), A12 (H2, H8, H1′, H2′, H4′, H5′/H5″), U16 (NH-3), G34 (2′-OH)
H5′/H5″	G8 (NH-1, NH_2-2), A12 (H2), U16 (NH-3)
A12	
NH_2-6	G17 (NH-1, NH_2-2), G34 (2′-OH)
H2	G11 (H4′, H5′/H5″), U16 (NH-3), G17 (NH-1)
H8	G11 (H4′), G34 (NH-1, H2′, 2′-OH)
H1′	G11 (H4′), G34 (NH-1, 2′-OH)
H2′	G11 (H4′), G34 (2′-OH)
H4′, H5′/H5″	G11 (H4′)
U16	
NH-3	A9 (H2), A10 (H1′, H2′, H3′), G11 (H4′, H5′/H5″), A12 (H2), G17 (NH-1)
H6	C15 (H5)
H1′, H2′, H3′	A9 (H2)
G17	
NH-1	A10 (H2), A12 (NH_2-6, H2), U16 (NH-3), U18 (NH-3), A33 (H2), G34 (NH-1, H8)
NH_2-2	A10 (H2), A12 (NH_2-6), U18 (NH-3), A33 (H2), G34 (H8)
H8, H2′, H3′	A9 (H2), A10 (H2)
H1′	A9 (H2), A10 (H2, H1′)
H4′, H5′/H5″	A9 (H2)
U18	
NH-3	G17 (NH-1, NH_2-2), G34 (H8)
A33	
H2	G17 (NH-1, NH_2-2), G34 (H8)
H8, H2′, H3′	G34 (NH-1)
G34	
NH-1	A12 (H8, H1′, H2′), G17 (NH-1), A33 (H8, H2′, H3′)
H8	G11 (NH-1), G17 (NH-1, NH_2-2), U18 (NH-3), A33 (H2)
H1′	G11 (NH-1)
2′-OH	G11 (H4′), A12 (NH_2-6, H8, H1′, H2′), A33 (H1′), G34 (H8, H1′, H2′, H3′, H4′, H5′/H5″)
H2′	A12 (H8)
C35	
H5	G11 (H8, H1′)
H6	G11 (NH-1, H1′)
H1′, H4′, H5′/H5″	G11 (NH-1)

[a] NOEs listed above are those observed in NOESY experiments in H_2O (100 ms mixing at 0 °C) and D_2O (120 ms mixing at 15 °C) for unlabeled RNA complexed with unlabeled AMP and confirmed in the 2D version of the (^1H,^{13}C) HMQC-NOESY experiment in H_2O (150 ms mixing at 0 °C) and the 3D (^1H,^{13}C) NOESY-HMQC experiment in D_2O (120 ms mixing at 30 °C) for uniformly ^{13}C,^{15}N-labeled RNA complexed with unlabeled AMP. NOEs detected only in the homonuclear experiment or only in the heteronuclear experiment are not listed.

residues (Table 2; see also dashed line connectivities in Figure 4a) that are indicative of stacking between G6 and G7 and between G11 and C35 in the complex. The observed strong NOE between the downfield-shifted imino proton of G7 and the H8 proton of G11 (peak k, Figure 2a) appears to be consistent with the formation of a G7·G11 mismatch involving the Watson−Crick edge of G7 and the Hoogsteen edge of G11 in the complex. The left helical stem segment which terminates with the G6·C35 Watson−Crick base pair must extend further through stacking with the G7·G11 mismatch pair in the complex.

The G11-A12-A13 Segment. The sequential base−sugar H1′ NOE traces exhibit a weak NOE at the G11−A12 step and a break in the connectivity at the A12−A13 step (Figure 5) suggestive of unusual conformations within the G11-A12-A13 segment in the complex.

It appears that the NOE patterns require the G11 and A12 bases to be orthogonal to each other such that the A12 base is positioned along and over the C4′−C5′ backbone of G11 in the complex. Specifically, NOEs are observed between the H2 proton of A12 and the H4′ and H5′/5″ protons of G11, while the H8 proton of A12 shows a NOE only to the H4′ proton of G11 in the complex (Table 2 and Supporting Information, Figure S5b). This alignment is facilitated by both G11 and A12 adopting predominantly C2′-endo sugar pucker conformations in the complex.

The large upfield chemical shifts observed for the H4′ proton (1.60 ppm) and the H5′/5″ protons (2.98/3.57 ppm) of G11 provide further support for the proposed positioning of the C4′-C5′ backbone of G11 under the purine ring of A12 in the complex.

The A13-A14-C15-U16-G17 Segment. We detect sequential base−sugar H1′ NOE connectivities within the A13−A14−C15−U16−G17 steps within the internal loop indicative of a right-handed stacked alignment adopted by this segment of the complex.

The A33-G34-C35 Segment. The G34 base with its syn glycosidic torsion angle and its C2′-endo sugar pucker exhibits a few NOEs to its 5′-flanking A33 residue but none to its 3′-flanking C35 residue in the complex (Table 2). This suggests that the stacking of G11 with C35 (see above) must disrupt the G34−C35 step while retaining stacking at the A33−G34 step in the complex. The observed strong NOE between the H2 of A33 and the H8 of G34 and between the H8 of A33 and the imino proton of G34 (Table 2 and Supporting Information, Figures S5a and S6) suggests that the purine rings of anti A33 and syn G34 must stack such that their six- and five-membered rings overlap with each other.

The observed NOEs from the imino proton and the downfield-shifted amino proton of G17 to the H8 proton of G34 suggest formation of a G17·G34 mismatch involving the Watson−Crick edge of G17 and the Hoogsteen edge of G34 in the complex (Supporting Information, Figure S7). The right helical stem segment that terminates with the U18·A33 Watson−Crick base pair appears to extend further through stacking with the G17·G34 mismatched pair based on the observation of a strong NOE between the imino protons of G17 and U18 in addition to the NOEs discussed above between A33 and G34 in the complex.

Long-Range NOEs between A9−A10 and U16−G17 Steps. The fold of the internal loop extending from G7 to G17 is defined in part by long-range NOEs identified between protons associated with the A9−A10 and U16−G17 steps

in the AMP−RNA aptamer complex. Specifically, the H1′ proton of G17 shows unusually strong NOEs to the H2 protons of A9 (peak b, Figure 5a) and A10 (peak c, Figure 5a) while the H1′ proton of U16 shows an equally strong NOE to the H2 proton of A9 (peak d, Figure 5a) in the complex. In addition, base to base proton NOEs are observed between the H8 proton of G17 and the H2 protons of A9 (peak E, Supporting Information, Figure S5a) and A10 (peak D, Supporting Information, Figure S5a) in the complex. These long-range NOEs require that the A9-A10 and U16-G17 segments be in close proximity and define the relative alignments of these two steps separated in sequence in the AMP−RNA aptamer complex. Most likely, the Watson−Crick edges (monitored by the adenine H2 proton) of the A9 and A10 residues [which are stacked on each other on the basis of observed NOEs between their H2 protons (peak B, Supporting Information, Figure S5a) and their H8 protons (peak A, Supporting Information, Figure S5a)] are in close proximity to the minor groove (monitored by the sugar H1′ proton) sugar−phosphate backbone of U16 and G17 in the complex.

Long-Range NOEs between G11−A12 and G34−C35 Steps. The spatial relationship between the G11 and A12 internal loop residues and the G34 bulge and adjacent C35 residues can be defined by long-range NOEs between the G11-A12 and G34-C35 segments in the AMP−RNA aptamer complex.

We have already shown that G11 and C35 stack on each other on the basis of the extensive NOEs observed between these two residues in the complex. The A12 and G34 bases appear to also stack on each other on the basis of NOEs between the base and sugar protons of these residues in the complex (Table 2). The long axes of these stacked purine bases appear to be near orthogonal to each other with the H8 proton of A12 positioned proximal to the sugar ring of G34. The slow exchange and downfield shift of the 2′-OH proton of G34 could reflect hydrogen bonding to the N7 of A12 (peaks R and S, Figure 2a). This would be consistent with the NOE detected between the 2′-OH of G34 and the H8 (peak j, Figure 2a) and NH_2-6 protons of A12 in the complex. This proposed stacking of A12 and G34 is further supported by the observation of a strong NOE between the H2 proton of A12 and the imino proton of G17 associated with the G17·G34 mismatch pair (Table 2, Supporting Information, Figure S7).

By contrast, no NOEs are observed between A12 and C35 residues in the complex. These data suggest that G11 and A12 (which have been shown above to be likely aligned in orthogonal planes) act as spacers between adjacent G34 and C35 residues with G11 stacked on C35 and A12 stacked on G34 in the complex.

The alignment of G11 relative to the G34−C35 step can also be defined by strong NOEs from the NH1 imino proton of G11 (labeled **5**) to the H1′ protons of G34 and C35 in the complex (Supporting Information, Figure S6). These NOEs place the Watson−Crick edge (contains the imino proton) of G11 proximal to the minor groove edges (contains the sugar H1′ protons) of G34 and C35 in the complex.

AMP Complexation Shifts. The AMP ligand has been monitored by recording two-dimensional [(^{1}H,^{13}C) HSQC, (^{1}H,^{15}N) HSQC, HCCH-COSY, HCCH-TOCSY] and three-dimensional [(^{1}H,^{13}C) NOESY-HMQC] NMR experiments on uniformly ^{13}C,^{15}N-labeled AMP (<10% excess) bound to unlabeled RNA aptamer **2**. These spectra exhibit resonances from both free and bound AMP, with the free AMP cross peaks clearly visible (despite the small excess of ligand) due to the favorable relaxation properties of the unbound ligand. The free and bound AMP cross peaks in the spectrum of the AMP−RNA aptamer complex could be easily distinguished following comparison with the corresponding data on uniformly ^{13}C,^{15}N-labeled AMP alone in solution.

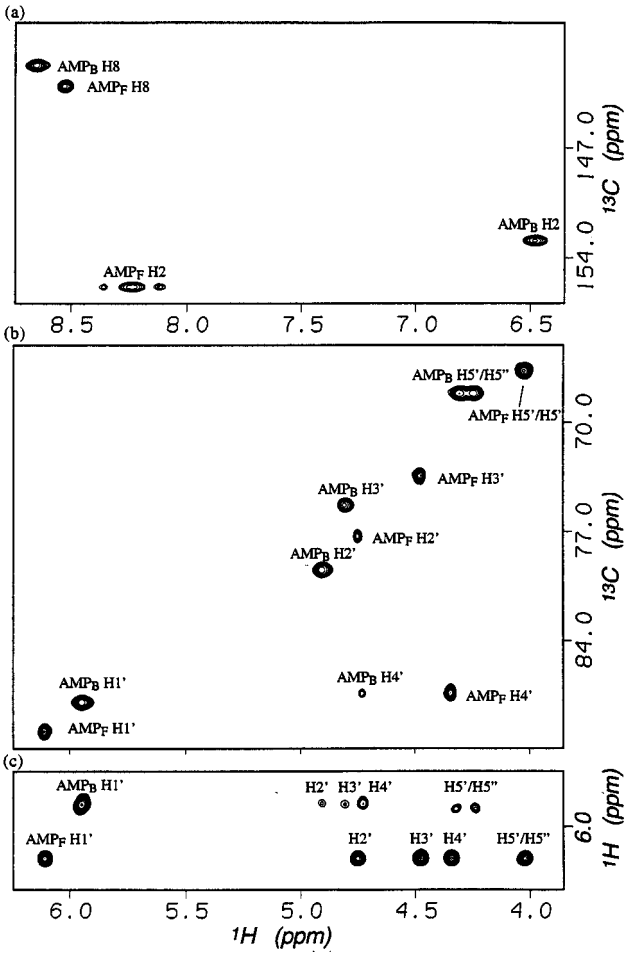

FIGURE 7: Contour plots of (a) the base region and (b) the sugar region of the ^{1}H−^{13}C plane of the (^{1}H,^{13}C) NOESY-HMQC experiment (optimized for sugar resonances) and (c) the H1′ to H2′-H5′/H5″ region of the (^{1}H,^{13}C) HCCH-TOCSY experiment for uniformly ^{13}C,^{15}N-labeled AMP (<10% excess) complexed with unlabeled RNA aptamer in D_2O buffer at 30 °C. The bound ligand is designated as AMP_B while the free ligand is designated as AMP_F. Although the amount of free ligand was small, the slower relaxation resulted in the observation of strong cross peaks for the free ligand. The sequential transfer of magnetization from the H1′ proton initially to the H2′ proton and subsequently all the way to the H5′/5″ protons can be clearly seen in (c). The H4′ and H5′ protons were identified from distinctive C4′ and C5′ carbon chemical shifts. The H2′ proton was identified from its COSY correlation to the H1′ proton in COSY experiments.

Expanded contour plots corresponding to the base region and sugar region associated with ^{1}H−^{13}C planes of the labeled AMP−RNA aptamer complex are plotted in panels a and b of Figure 7, respectively. Individual cross peaks are assigned in Figure 7 with free and bound forms identified by AMP_F and AMP_B, respectively. The corresponding HCCH-TOCSY experiment that correlates the H1′ proton with the other sugar protons on AMP_F and AMP_B in the complex is shown in Figure 7c.

The proton and carbon chemical shifts of free and bound AMP along with the chemical shift changes associated with

Table 3: ^{1}H, ^{13}C, and ^{15}N Chemical Shifts of the Ligand AMP in the Free State and When Bound to the RNA Aptamer[a]

AMP	free	bound	$\Delta\delta$
proton			
H2	8.24	6.49	−1.75
H8	8.52	8.65	+0.13
H1′	6.11	5.95	−0.16
H2′	4.75	4.91	+0.16
H3′	4.48	4.81	+0.33
H4′	4.34	4.73	+0.39
H5′,H5″	4.03	4.25, 4.31	+0.22, 0.28
NH_2-6	6.85	6.86, 7.78	+0.01, 0.93
carbon-13			
C2	156.0	153.1	−2.9
C8	143.1	141.7	−1.4
C1′	89.8	88.0	−1.8
C2′	77.1	79.3	+2.2
C3′	73.2	75.1	+1.9
C4′	87.3	87.4	+0.1
C5′	66.3	67.7	+1.4
nitrogen-15			
N-6	79.9	85.4	+5.5

[a] Chemical shifts of exchangeable protons and nitrogens for both free and bound AMP are obtained from the (^{1}H,^{15}N) HSQC experiment (0 °C) and those of nonexchangeable protons and carbons from the (^{1}H,^{13}C) NOESY-HMQC experiment (30 °C) on uniformly ^{13}C,^{15}N-labeled AMP bound to the RNA aptamer in 10 mM sodium phosphate and 0.2 mM EDTA, pH 6.7.

AMP−RNA aptamer complex formation are listed in Table 3. A large upfield shift is observed at the base H2 proton (−1.75 ppm), and smaller downfield shifts are observed at the sugar H3′ (+0.33 ppm) and H4′ (+0.39 ppm) protons of AMP on complex formation (Table 3). The H5′,5″ protons of AMP are superpositioned in the free ligand but exhibit a very small chemical shift nonequivalence for the bound ligand in the AMP−RNA aptamer complex.

Complexation shifts are also detected at the carbon resonances of AMP with the largest difference being a −2.9 ppm upfield shift for the base C2 carbon on AMP−RNA aptamer complex formation (Table 3).

The exocyclic amino protons of AMP have also been followed on AMP−RNA aptamer complex formation. The two amino protons are superpositioned in free AMP, but one of them exhibits a large downfield shift (+0.93 ppm) on complex formation (Table 3). This strongly suggests that one of the amino protons participates in an intermolecular hydrogen bond on complex formation. We also note that the exocyclic amino nitrogen also undergoes a downfield shift (+5.5 ppm) on complex formation (Table 3).

AMP Sugar Pucker. The sugar proton coupling constant data are consistent with a predominant C2′-endo sugar pucker for AMP in the free state and, to a lesser extent, when bound to the RNA aptamer. Thus, a strong H1′−H2′ coupling cross peak is detected for AMP_F and a weaker counterpart is detected for AMP_B in the COSY spectrum of the AMP−RNA aptamer complex (Supporting Information, Figure S4).

Intermolecular NOEs Involving AMP Base Protons. The available assignments of both the bound AMP and the RNA aptamer protons in turn permit the identification and assignment of intermolecular NOEs in the AMP−RNA aptamer complex (Table 4). These intermolecular NOEs were identified initially following analysis of homonuclear NOESY spectra of the complex in H_2O and D_2O solution. This identification was greatly facilitated following analysis of the two-dimensional version of the (^{1}H,^{13}C) HMQC-NOESY experiment in H_2O solution and the three-dimensional (^{1}H,^{13}C) NOESY-HMQC experiment in D_2O solution on the AMP−RNA aptamer complex which was uniformly ^{13}C,^{15}N-labeled on either the AMP or the RNA.

Table 4: Intermolecular NOEs between AMP and the RNA Aptamer in the AMP−RNA Aptamer Complex[a]

AMP	
H2	G8 (NH-1, NH_2-2), A10 (H2, H8, H1′, H2′, H3′, H4′, (H5′/H5″), A12 (H2), G11 (H8, H1′, H4′, H5′/H5″)
H8	A10 (H2), G11 (NH-1), U18 (H1′)
H1′	A10 (H2), G11 (NH-1), G17 (NH-1, NH_2-2), U18 (H1′, H4′), G34 (H8, H1′, 2′-OH)
H2′	G17 (NH_2-2), U18 (H1′, H4′)
H3′	G17 (NH_2-2), U18 (H1′, H4′)
H4′	G11 (NH-1), U18 (H1′, H4′), G34 (H8, H1′)

[a] NOEs listed were observed in NOESY experiments in H_2O (100 ms mixing at 0 °C) and D_2O (120 ms mixing at 15 °C) for the unlabeled RNA−AMP complex. They were confirmed in the two-dimensional version of the (^{1}H,^{13}C) HMQC-NOESY experiment in H_2O (150 ms mixing at 0 °C) and the (^{1}H,^{13}C) NOESY-HMQC in D_2O (350 ms mixing at 30 °C) for unlabeled RNA complexed with uniformly ^{13}C,^{15}N-labeled AMP or uniformly ^{13}C,^{15}N-labeled RNA complexed with unlabeled AMP. NOEs detected only in the high-sensitivity homonuclear experiment are not listed.

The H2 proton of bound AMP at 6.49 ppm exhibits a large number of intermolecular NOEs to the base and sugar protons of A10 and G11 in expanded NOESY (250 ms mixing time) contour plots of the complex in D_2O solution at 15 °C (Figure 8a). The strongest intermolecular NOEs among the nonoverlapped cross peaks are to the sugar H1′, H2′, and H3′ protons of A10 and the H4′ proton of G11 in the complex (Figure 8a). These data suggest that the purine ring of AMP is most likely sandwiched between the purine planes of A10 and G11 of the RNA aptamer in the complex.

The H8 proton of bound AMP at 8.65 ppm exhibits NOEs to the H2 proton of A10 and the NH1 imino proton of G11 in the AMP−RNA aptamer complex (Table 4). These data imply that the five-membered ring of AMP (from which projects the H8 proton) most likely stacks between the six-membered rings of A10 and G11 (from which project the imino and H2 protons) in the complex.

The H2 proton of bound AMP also exhibits NOEs to the imino and hydrogen-bonded amino protons of G8 with a stronger NOE to the latter exchangeable proton in the complex. These data are suggestive of an in-plane alignment between the purine bases of AMP and G8 with the minor groove amino group containing edge of G8 most likely involved in AMP recognition.

Intermolecular NOEs Involving AMP Sugar Protons. We observe a range of intermolecular NOEs from the sugar protons of bound AMP to the base and sugar protons of A10, G11, G17, U18, and G34 in the AMP−RNA aptamer complex (Table 4). Some of these intermolecular NOEs are shown in strip contour plots associated with the C1′, C2′, C3′, and C4′ planes taken from a three-dimensional (^{1}H,^{13}C) NOESY-HMQC experiment on uniformly ^{13}C,^{15}N-labeled AMP bound to unlabeled RNA aptamer in D_2O buffer at 30 °C (Figure 8b). These include protons distributed along the Watson−Crick edge of A10 (H2 proton), G11 (NH1 proton), and G17 (NH1 and NH_2-2 protons) and the minor groove edges of U18 (H1′ and H4′ protons) and G34 (H1′ and 2′-OH protons) in the complex. In addition, a strong NOE is observed between the H1′ and H4′ protons of AMP and the Hoogsteen edge of G34 (H8 proton) in the complex. These intermolecular NOEs suggest that the sugar ring of AMP is positioned over the minor groove of the right helical segment

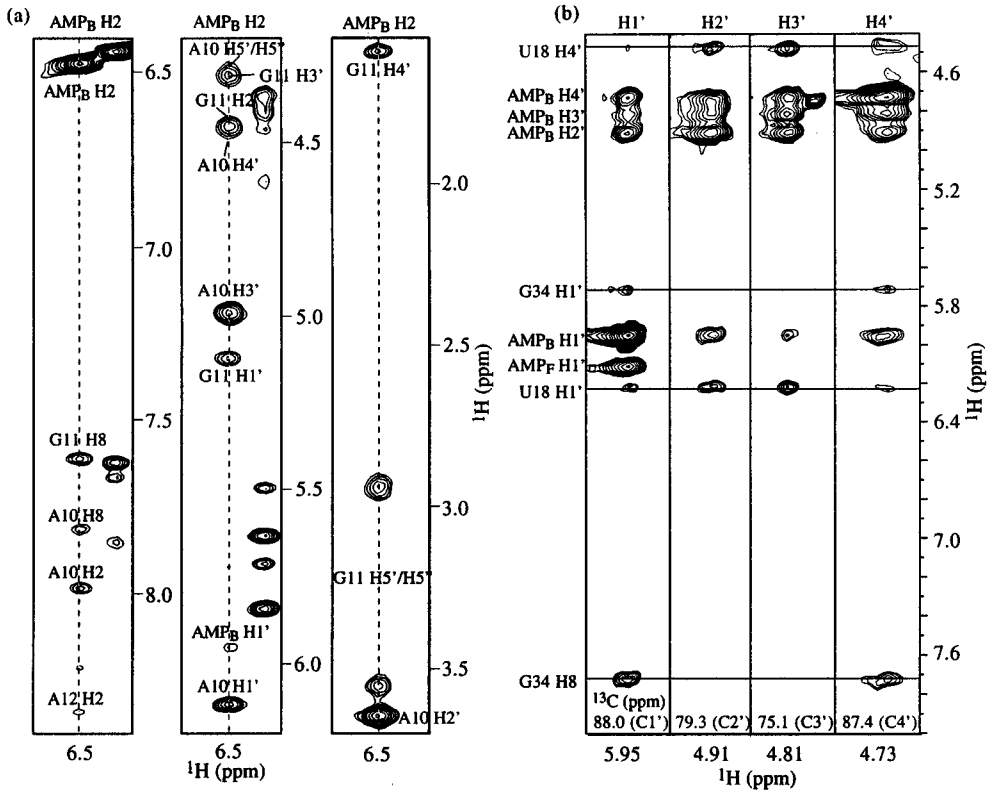

FIGURE 8: (a) Expanded contour plots of the NOESY spectrum (250 ms mixing time) for the unlabeled RNA aptamer complexed to unlabeled AMP in D_2O buffer, pH 6.7 at 15 °C, showing NOEs from the AMP(H2) proton to the RNA protons. (b) Strip plots of the NOESY-HMQC experiment (350 ms mixing time) in D_2O buffer, pH 6.7 at 30 °C, for unlabeled RNA aptamer complexed with uniformly ^{13}C,^{15}N-labeled AMP showing NOEs between AMP sugar protons and RNA protons. The NOEs from AMP$_B$(H1′) to G34(H8, H1′) and U18(H1′, H4′) can also be identified in strips of the G34(C8, C1′) and U18(C1′, C4′) planes from a (^{1}H,^{13}C) NOESY-HMQC experiment on unlabeled AMP complexed with the uniformly ^{13}C,^{15}N-labeled RNA aptamer. Due to the downfield shift of the U18(H1′) proton, NOEs from U18(H1′) to AMP(H2′, H3′) can be confirmed in higher resolution homonuclear NOESY experiments. However, the NOEs from U18(H4′) to AMP(H2′, H3′) cannot be confirmed by either NOESY or NOESY-HMQC experiments due to the overlap of U18(H4′) with other sugar protons in the 2D spectrum or the overlap of AMP$_B$(H2′, H3′, H4′) with U18(H2′) at 4.86 ppm and U18(H3′) at 4.71 ppm in the 3D spectra. Similarly, NOEs from AMP$_B$(H4′) to G34(H1′, H4′) remain to be confirmed.

(U18 to C23 and G28 to A33) which is extended beyond the U18·A33 base pair by the G17·G34 mismatch pair in the folded conformation of the RNA aptamer in the complex.

NOE Distribution in the Complex. The distribution and schematic drawing of long-range NOEs within the internal loop and bulge and flanking base pairs (G6 to U18 and A33 to C35 segments) of RNA aptamer **2** together with the intermolecular NOEs involving this RNA segment and AMP in the complex are shown in panels a and b of Figure 9, respectively. It is readily apparent from this figure that the key intermolecular contacts are made between AMP and residues A10, G11, G17, U18, and G34 in the complex. Specific features of the folding topology of the internal loop and bulge of the RNA aptamer and the AMP binding pocket implicit in these schematics of the complex are evaluated in the Discussion section below.

DISCUSSION

Our ability to assign the base and sugar proton resonances of the consensus 11 base G7 to G17 internal loop, the invariant G34 bulge base, and the flanking G6·C35 and U18·A33 base pairs of RNA aptamer **2** (Table 1) together with the proton assignments of the bound AMP (Table 3) in the complex has allowed us to identify the intramolecular (Table 2) and intermolecular (Table 4) NOEs that are a prerequisite for characterization of structural insights into the RNA fold and AMP−RNA molecular recognition. We outline below the structural insights that have emerged related to folding and recognition in the AMP−RNA aptamer complex. These qualitative conclusions based on an analysis of the NMR data (this study) are further verified and elaborated upon in quantitative detail in the solution structure of the AMP−RNA aptamer complex deduced from molecular dynamics computations guided by the NMR restraints (Jiang et al., 1996a).

G·G Mismatch Formation. We have identified G·G mismatch formation for G7·G11 and G17·G34 pairs in the AMP−RNA aptamer complex. The G7(*anti*)·G11(*anti*) mismatch pair is of the reverse Hoogsteen type (Figure 10a) and has been characterized on the basis of an NOE between the imino proton of G7 and the H8 proton of G11 and additional NOEs to the adjacent G8 residue and G6·C35 Watson−Crick base pair in the complex. The downfield shift of the imino proton of G7 (13.24 ppm) reflects potential hydrogen bond formation with the N7 ring nitrogen of G11 while the upfield shift of the imino proton of G11 (10.41 ppm) establishes that it is not hydrogen bonded in the complex (Figure 10a).

The G17(anti)·G34(syn) mismatch pair is of the Hoogsteen type (Figure 10b) and has been characterized on the basis of NOEs from the imino and downfield-shifted 9.12 ppm amino proton of G17 to the H8 proton of G34 and additional NOEs to the adjacent A12 residue and U18·A33 Watson−Crick base pair in the complex. The 11.06 ppm imino proton shift of G17 (reflecting potential hydrogen bonding to the carbonyl group of G34) is downfield of the 10.33 ppm non-

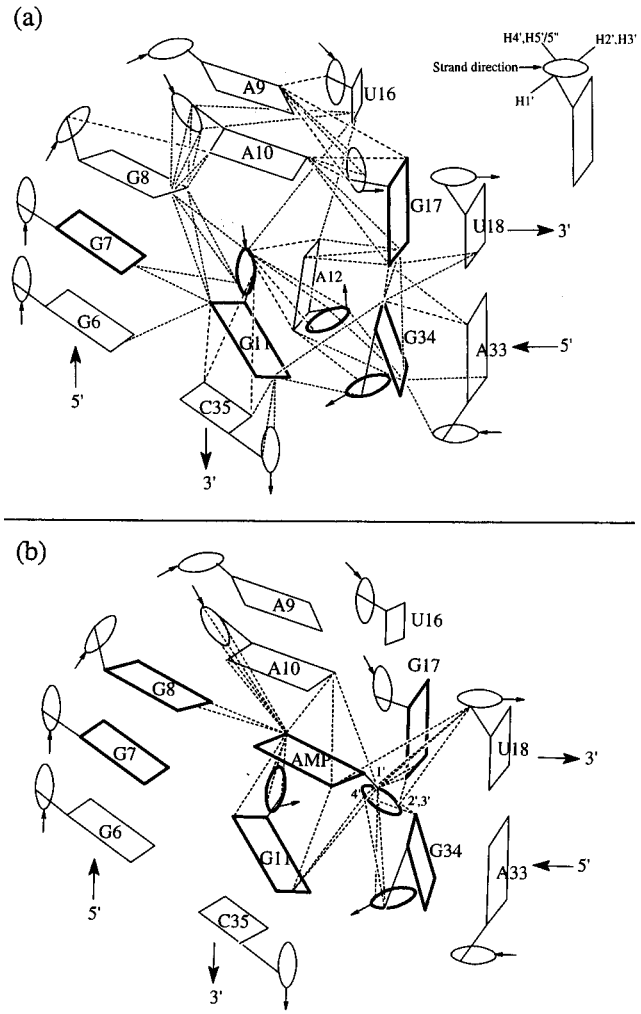

FIGURE 9: Schematic drawing of (a) unusual NOEs within the internal loop and bulge segments of RNA and (b) intermolecular NOEs between AMP and the internal loop and bulge segments of RNA in the AMP−RNA aptamer complex. Residues A13 to C15 have been omitted from (a) and residues A12 to C15 from (b) for clarity. The bases involved in mismatch formation are shown in thick lines. The sugars adopting C2′-endo pucker are shown in thick lines.

hydrogen-bonded imino proton of G34 in the complex (Figure 10b). The downfield shift of one amino proton of G17 to 9.12 ppm reflects its potential participation with the N7 ring nitrogen of G34 in the complex (Figure 10b).

Extension of the Helical Stems into the Internal Loop and Bulge Segments. The stacking of internal loop and bulge residues with adjacent Watson−Crick helical stem segments represents a key element in generating the AMP binding fold of RNA aptamer **2**. The NOE and chemical shift patterns indicate that the leftward stem is extended through stacking of the G7(anti)·G11(anti) reverse Hoogsteen mismatch pair (Figure 10a) with the Watson−Crick G6·C35 pair in one direction and stacking of G8 with G7 of the G7·G11 mismatch pair in the opposite direction (Figure 9a). Similarly, the rightward stem is extended through stacking of the G17(anti)·G34(syn) Hoogsteen mismatch pair (Figure 10b) with the Watson−Crick U18·A33 pair in one direction and stacking of A12 with G34 of the G17·G34 mismatch pair in the opposite direction (Figure 9a). The potential orthogonal alignment of the G11 and A12 bases suggests that the respective extended stems to which they belong will also adopt an approximate orthogonal alignment in the complex.

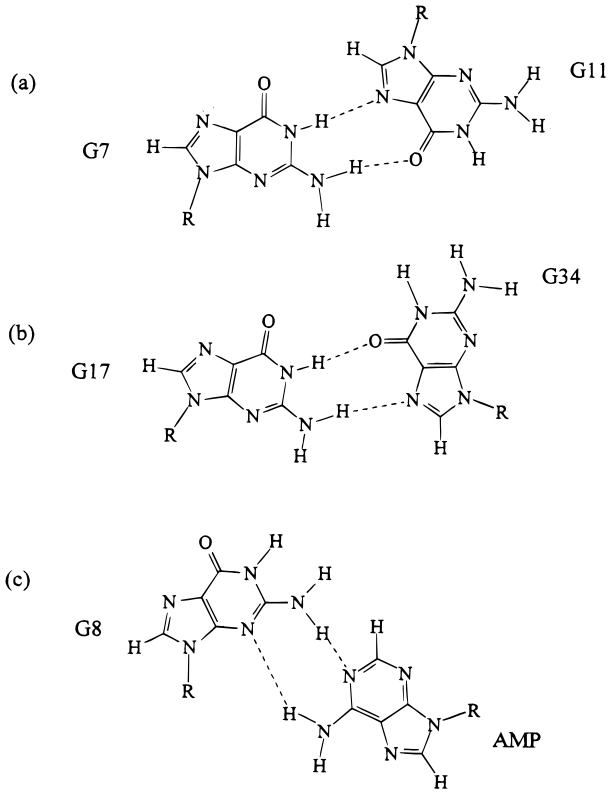

FIGURE 10: Potential hydrogen-bonding alignments for (a) the G7·G11, (b) the G17·G34, and (c) intermolecular G8·AMP pairs in the AMP−RNA aptamer complex.

Chain Reversal Encompassing the G7 to G11 Internal Loop Segment. The G7 to G11 segment of the internal loop adopts an unexpected fold defined by a chain reversal centered about the G8−A9 step, participation of the purine ring of AMP in the fold, and tethering the ends of the segment through G7·G11 mismatch formation in the complex (Figure 9b). A key feature of this all-purine fold is the stacking interactions between G7 and G8 and the extended sequential stacking of A9, A10, AMP, and G11 along the chain (Figure 9b). The very few NOEs between G8 and A9 (Table 2) reflect the stacking discontinuity associated with chain reversal at the G8−A9 step in the complex. The intercalation of the purine ring of AMP between A10 and G11 in the complex represents an unprecedented participation of the aromatic ring of a cofactor in filling a gap necessary to achieve reversal of the nucleotide chain. It has not escaped our notice that there are parallels between the stacking patterns reported for GNRA RNA hairpin loops (Heus & Pardi, 1991; Orita et al., 1993; Pley et al., 1994) and the present observation of a G8-A9-A10-AMP hairpin loop closed by the G·G mismatch in the AMP−RNA aptamer complex.

Stacking within the A13 to U16 Internal Loop Segment. The bound AMP ligand exhibits a single very weak intermolecular NOE to the A13-A14-C15-U16 segment of the internal loop in the AMP−RNA aptamer complex. This contrasts with AMP exhibiting several intermolecular NOEs to the A10, G11, G17, U18, and G34 residues in the complex (Table 4). This implies that the A13-A14-C15-U16 internal loop segment does not form part of the binding pocket for AMP in the complex. Our NMR data are consistent with AMP intercalation into a binding pocket generated primarily by the A10, G11, A12, G17, and G34 internal loop and bulge residues along one face of the RNA aptamer, and it is conceivable that the internal loop A13-A14-C15-U16 seg-

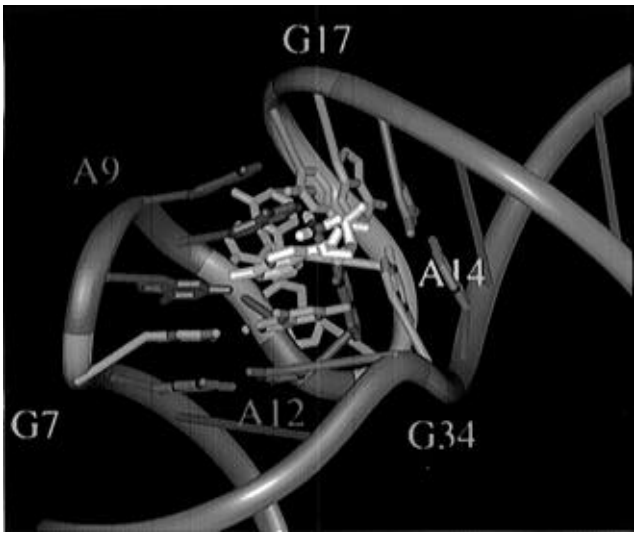

FIGURE 11: Ribbon representation of a representative solution structure of the AMP−RNA aptamer complex (Jiang et al., 1996) using the Insight (Biosym/MSI) program. The bases for the G6 to U18 and A33 to C35 residues are shown in a stick representation. The G7·G11 and G17·G34 mismatches are colored mustard, the G8-G9-A10 segment involved in a GNRA hairpin loop is colored magenta, the central A12 residue is colored rusty red, the A13-A14-C15-U16 segment that closes the back of the binding site is colored yellow, and the bound AMP is in white except for its phosphate which is in red. The left helical stem is colored cyan while the right helical stem is colored green.

ment in a stacked alignment (based on sequential NOE connectivities) caps the opposite face of the RNA aptamer in the complex.

Thus, it appears that the A13 to U16 segment is not directly involved in the AMP recognition but contributes to the generation of the RNA scaffold necessary for generating the AMP binding site. Consistent with this proposal is the observation that the A13 to U16 segment constitutes the most variable region within the 11 base internal loop among the RNA aptamer sequences identified for their ability to target AMP in the *in vitro* selection experiments (Sassanfar & Szostak, 1993).

AMP Intercalation into the A10−G11 Step. The purine ring of AMP intercalates between A10 and G11 in the complex (Figure 9b) with extensive stacking between adjacent purine rings as reflected in the upfield shifts of the H2 proton of AMP on complex formation. The observed distribution of NOEs between the AMP protons and those of A10 and G11 (Table 4) suggests that the fused five- and six-membered rings of AMP stack predominantly with the fused six- and five-membered rings, respectively, of the flanking A10 and G11 residues in the complex.

Intermolecular AMP·G8 Pairing Alignment. The recognition of AMP by the RNA aptamer is associated with the alignment of the Watson−Crick edge of AMP with the minor groove edge of G8 in the complex. The amino protons of both AMP and G8 could potentially participate in mutual NH_2 donor to ring nitrogen acceptor hydrogen bond alignments as shown in Figure 10c. The chemical shifts of the imino and amino protons of AMP and G8 are consistent with such an alignment in the complex. Thus, the 10.72 ppm imino proton chemical shift of G8 is typical of a nonpairing alignment while the amino proton chemical shifts of G8 (5.03 and 8.84 ppm) and AMP (6.86 and 7.78 ppm) suggest that the downfield-shifted member of each amino proton pair could participate in hydrogen bond formation associated with the recognition process (Figure 12b).

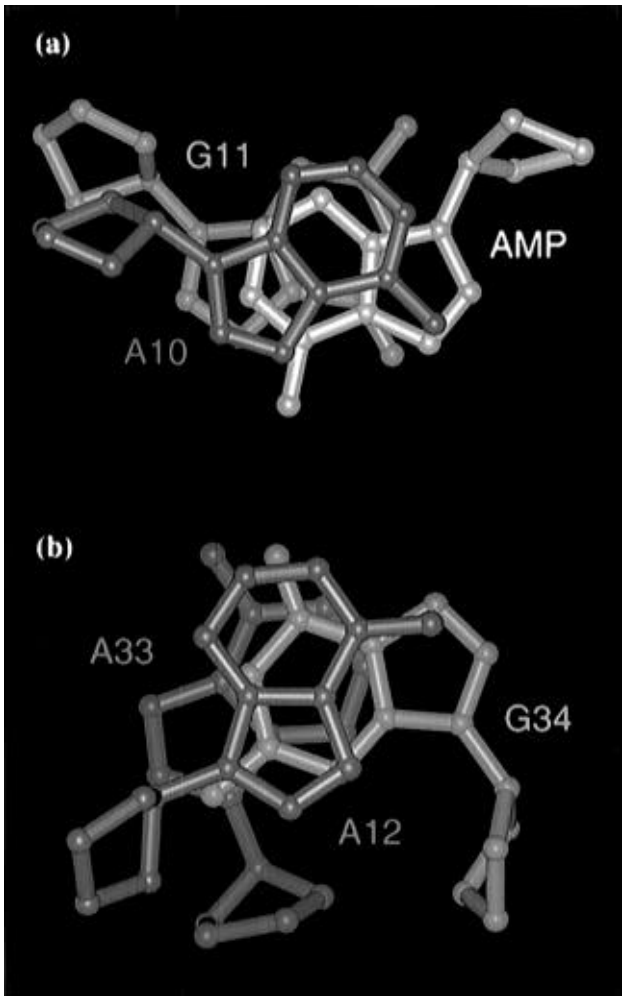

FIGURE 12: (a) Base stacking of AMP (in white) with sequentially flanking A10 (in magenta) and G11 (in mustard) residues and (b) base stacking of G34 (in mustard) with spatially flanking A12 (in rusty red) and sequentially flanking A33 (in green) residues in one representative refined structure of the AMP−RNA aptamer complex (Jiang et al., 1996a).

Further, the orthogonal arrangement of the purine ring planes of the A10-AMP-G11 segment and the A12 residue, when coupled with the Watson−Crick edge of A12 being directed toward the minor groove of the bound AMP, opens the possibility of an additional hydrogen bond forming between the exocyclic amino group of A12 and the N3 position of the purine ring of AMP in the complex. Molecular recognition would then involve hydrogen bond participation of the N1, N3, and NH_2-6 positions on AMP, leaving only the N7 position uninvolved in recognition due to its proximity to the C8 position through which the cofactor was covalently attached to the column for screening of the random RNA library.

Solution Structure of the AMP−RNA Aptamer Complex. Our group has recently published the solution structure of the AMP−RNA aptamer complex (Jiang et al., 1996a) based on molecular dynamics calculations guided by NMR-based intramolecular and intermolecular restraints outlined in this paper. A ribbon view of the RNA fold of the G7 and G17 internal loop, the G34 bulge, and the bound AMP in one representative refined structure of the complex (Jiang et al., 1996a) is shown in color in Figure 11. The core of this structure is composed of two sets of stacked purine arrays as exemplified by the bound AMP which is stacked between A10 and G11 (Figure 12a) and the bulged G34 in a syn

orientation which is stacked between A33 and A12 (Figure 12b) in the complex. The structural insights related to RNA folding, mismatch alignment, base stacking, and molecular recognition (Figures 9 and 10) proposed on the basis of a qualitative analysis of the NOE and chemical shift information outlined in this paper have been verified in the high-resolution refined structure of the AMP−RNA aptamer complex (Figures 11 and 12) reported recently from our laboratory (Jiang et al., 1996a).

ACKNOWLEDGMENT

F.J. thanks Drs. Nancy Greenbaum, David Hirsh, Anna Maria Pyle, and Wei-jun Xu and staff in the Hirsh laboratory for helpful suggestions and technical assistance in preparing the initial RNA samples.

SUPPORTING INFORMATION AVAILABLE

Three tables listing acquisition parameters for multidimensional NMR experiments, imino proton and nitrogen chemical shifts in the free RNA, and the AMP−RNA complex and proton, carbon, and phosphorus chemical shifts in stem and hairpin loop segments in the complex and seven figures identifying amino protons in the (^{1}H,^{15}N) HSQC experiment, sugar proton coupling correlations in (^{1}H,^{13}C) HCCH-COSY and phase-sensitive COSY experiments, and NOE connectivities between nonadjacent residues in NOESY and between imino protons and base and sugar protons in (^{1}H,^{13}C) HMQC-NOESY experiments (17 pages). Ordering information is given on any current masthead page.

REFERENCES

Allain, F. H.-T., & Varani, G. (1995) *J. Mol. Biol. 250*, 333−353.
Bax, A., & Davis, D. G. (1985) *J. Magn. Reson. 65*, 355−360.
Bax, A., Clore, G. M., Driscoll, P. C., Gronenborn, A. M., Ikura, M., & Kay, L. E. (1990) *J. Magn. Reson. 87*, 620−627.
Boelens, R., Scheek, R. M., Dijkstra, K., & Kaptein, R. (1985) *J. Magn. Reson. 62*, 378−386.
Burgstaller, P., & Famulok, M. (1995) *Angew. Chem., Int. Ed. Engl. 34*, 1189−1192.
Chapman, K. B., & Szostak, K. W. (1994) *Curr. Opin. Struct. Biol. 4*, 618−622.
Cheong, C., Varani, G., & Tinoco, I., Jr. (1990) *Nature 346*, 680−682.
Clore, G. M., Bax, A., Driscoll, P. C., Winhfield, P. T., & Gronenborn, A. M. (1990) *Biochemistry 29*, 8172−8184.
Davanloo, P., Rosenberg, A. H., Dunn, J. J., & Studier, F. W. (1984) *Proc. Natl. Acad. Sci. U.S.A. 81*, 2035−2039.
Delaglio, F., Grzesiek, S., Vuister, G., Zu, G., Pfeiffer, J., & Bax, A. (1995) *J. Biomol. NMR 6*, 277−293.
Ellington, A., & Szostak, J. W. (1990) *Nature 346*, 818−822.
Fan, P., Suri, A. K., Fiala, R., Live, D., & Patel, D. J. (1996) *J. Mol. Biol. 258*, 480−500.
Fesik, S. W., & Zuiderweg, E. R. P. (1988) *J. Magn. Reson. 78*, 588−593.
Fesik, S. W., Eaton, H. L., Olejniczak, E. T., Zuiderweg, E. R. P., McIntosh, L. P., & Dahlquist, F. W. (1990) *J. Am. Chem. Soc. 112*, 886−888.
Fiala, R., Jiang, F., & Patel, D. J. (1996) *J. Am. Chem. Soc. 118*, 689−690.
Garret, D. S., Powers, R., Gronenborn, A., & Clore, G. M. (1991) *J. Magn. Reson. 95*, 214−220.
Gesteland, R., & Atkins, J., Eds. (1993) *The RNA World*, Cold Spring Harbor Press, Cold Spring Harbor, NY.
Ghose, R., Marino, J. P., Wiberg, K. B., & Prestegard, J. H. (1994) *J. Am. Chem. Soc. 116*, 8827−8828.
Greenbaum, N., Radhakrishnan, I., Hirsh, D., & Patel, D. J. (1995) *J. Mol. Biol. 252*, 314−327.
Greene, K. L., Wang, Y., & Live, D. (1995) *J. Biomol. NMR 5*, 333−338.
Heus, H. A., & Pardi, A. (1991) *Science 253*, 191−194.
Huizenga, D. E., & Szostak, J. W. (1995) *Biochemistry 34*, 656−665.
Jiang, F., Kumar, R. A., Jones, R., & Patel, D. J. (1996a) *Nature 382*, 183−186.
Jiang, F., Patel, D. J., Zhang, X., Zhao, H., & Jones, R. A. (1996b) *J. Biomol. NMR* (submitted for publication).
Joyce, G. F. (1994) *Curr. Opin. Struct. Biol. 4*, 331−336.
Kay, L. E., Keifer, P., & Saarinen, T. (1992) *J. Am. Chem. Soc. 114*, 10663−10665.
Kellogg, G. W., & Schweitzer, B. I. (1993) *J. Biomol. NMR 3*, 577−595.
Legault, P., Farmer, B. T., II, Muller, L., & Pardi, A. (1994) *J. Am. Chem. Soc. 116*, 2203−2204.
Lorsch, J. R., & Szostak, J. W. (1994) *Nature 371*, 31−36.
Mao, B., Cosman, M., Hingerty, B. E., Broyde, S., & Patel, D. (1995) *Biochemistry 34*, 6226−6238.
Marino, J. P., Prestegard, J. H., & Crothers, D. M. (1994) *J. Am. Chem. Soc. 116*, 2205−2206.
Marion, D., Ikura, M., Tschudin, R., & Bax, A. (1989) *J. Magn. Reson. 85*, 393−399.
Milligan, J. F., & Uhlenbeck, O. C. (1989) *Methods Enzymol. 180*, 51−62.
Milligan, J. F., Groebe, D. R., Witherell, G. W., & Uhlenbeck, O. C. (1987) *Nucleic Acids Res. 15*, 8783−8789.
Moore, P. B. (1995) *Acc. Chem. Res. 28*, 251−256.
Nagai, K., & Mattaj, I. W., Eds. (1994) *RNA−Protein Interactions*, IRL Press, Oxford.
Nikonowicz, E. P., Sirr, A., Legault, P., Jucker, F. M., Baer, L. M., & Pardi, A. (1992) *Nucleic Acids Res. 20*, 4508−4513.
Orita, M., Nishikawa, F., Shimayama, T., Taira, K., Endo, Y., & Nishikawa, S. (1993) *Nucleic Acids Res. 21*, 5670−5678.
Pardi, A. (1995) *Methods Enzymol. 261*, 350−380.
Patel, D. J., Kozlowski, S. A., Nordheim, A., & Rich, A. (1982) *Proc. Natl. Acad. Sci. U.S.A. 79*, 1413−1417.
Patel, D. J., Shapiro, L., & Hare, D. (1987) *Q. Rev. Biophys. 20*, 35−112.
Plateau, P., & Gueron, M. (1982) *J. Am. Chem. Soc. 104*, 7310−7311.
Pley, H. W., Flahorty, K. M., & McKay, D. B. (1994) *Nature 372*, 111−113.
Robertson, D. L., & Joyce, G. F. (1990) *Nature 344*, 467−468.
Santoro, J., & King, G. C. (1992) *J. Magn. Reson. 97*, 202−207.
Sassanfar, M., & Szostak, J. W. (1993) *Nature 364*, 550−553.
Shaka, A. J., Barker, P. B., & Freeman, R. (1985) *J. Magn. Reson. 64*, 547−552.
Shaka, A. J., Lee, C. J., & Pines, A. (1988) *J. Magn. Reson. 77*, 274−293.
Simorre, J. P., Zimmermann, G. R., Mueller, L., & Pardi, A. (1996) *J. Biomol. NMR 7*, 153−156.
Sklenar, V., Myashiro, H., Zon, G., Miles, H. T., & Bax, A. (1986) *FEBS Lett. 208*, 94−98.
Sklenar, V., Dieckmann, T., Butcher, S. F., & Feigon, J. (1996) *J. Biomol. NMR 7*, 83−87.
Smallcombe, S. H. (1993) *J. Am. Chem. Soc. 115*, 4776−4785.
States, D. J., Haberkorn, R. A., & Ruben, D. J. (1982) *J. Magn. Reson. 48*, 286−292.
Tuerk, C., & Gold, L. (1990) *Science 249*, 505−510.
Varani, G., Cheong, C., & Tinoco, I., Jr. (1991) *Biochemistry 30*, 3280−3289.
Vuister, G. W., & Bax, A. (1992) *J. Magn. Reson. 98*, 428−435.
Wang, Y., de los Santos, C., Gao, X., Greene, K., Live, D., & Patel, D. J. (1991) *J. Mol. Biol. 222*, 819−832.
Wishart, D. S., Bigam, C. G., Yao, J., Abildgaad, F., Dyson, H. J., Oldfield, E., Markley, J. L., & Sykes, B. D. (1995) *J. Biomol. NMR 6*, 135−140.
Wyatt, J. R., & Tinoco, I., Jr. (1993) in *The RNA World* (Gesteland, R. F., & Atkins, J. F., Eds.) pp 465−496, Cold Spring Harbor Laboratory Press, Cold Spring Harbor, NY.
Wyatt, J. R., Chastain, M., & Puglisi, J. D. (1991) *BioTechniques 11*, 764−769.
Zuiderweg, E. R. P., McIntosh, L. P., Dahlquist, F. W., & Fesik, S. W. (1990) *J. Magn. Reson. 86*, 210−216.

BI961345Q